DISEASES AND DISORDERS

Actin-binding protein filamin-A drives tau aggregation and contributes to progressive supranuclear palsy pathology

Koyo Tsujikawa[1,2,3], Kohei Hamanaka[4], Yuichi Riku[1,5], Yuki Hattori[6], Norikazu Hara[7], Yohei Iguchi[1], Shinsuke Ishigaki[1,8], Atsushi Hashizume[1,9], Satoko Miyatake[4,10], Satomi Mitsuhashi[4,11], Yu Miyazaki[1], Mayumi Kataoka[1], Li Jiayi[1], Keizo Yasui[2], Satoshi Kuru[3], Haruki Koike[1], Kenta Kobayashi[12], Naruhiko Sahara[13], Norio Ozaki[14], Mari Yoshida[5], Akiyoshi Kakita[15], Yuko Saito[16], Yasushi Iwasaki[5], Akinori Miyashita[7], Takeshi Iwatsubo[17], Japanese Alzheimer's Disease Neuroimaging Initiative (J-ADNI)†, Takeshi Ikeuchi[7], Japanese Longitudinal Biomarker Study in PSP and CBD (JALPAC) Consortium‡, Takaki Miyata[6], Gen Sobue[8], Naomichi Matsumoto[4], Kentaro Sahashi[1], Masahisa Katsuno[1,9]*

While amyloid-β lies upstream of tau pathology in Alzheimer's disease, key drivers for other tauopathies, including progressive supranuclear palsy (PSP), are largely unknown. Various tau mutations are known to facilitate tau aggregation, but how the nonmutated tau, which most cases with PSP share, increases its propensity to aggregate in neurons and glial cells has remained elusive. Here, we identified genetic variations and protein abundance of filamin-A in the PSP brains without tau mutations. We provided in vivo biochemical evidence that increased filamin-A levels enhance the phosphorylation and insolubility of tau through interacting actin filaments. In addition, reduction of filamin-A corrected aberrant tau levels in the culture cells from PSP cases. Moreover, transgenic mice carrying human filamin-A recapitulated tau pathology in the neurons. Our data highlight that filamin-A promotes tau aggregation, providing a potential mechanism by which filamin-A contributes to PSP pathology.

INTRODUCTION

Progressive supranuclear palsy (PSP) is a pathologically defined tauopathy with a broad clinical spectrum ranging from abnormal movement predominant types (e.g., classical Richardson's syndrome and PSP parkinsonism) to abnormal behavioral predominant types (e.g., PSP with frontotemporal dementia) (*1*). PSP is not rare and has prevalence of 18 cases per 100,000 in both the United Kingdom and Japan (*1*). Patients usually die in 5 to 10 years after onset because of the lack of effective treatment, and their serious physical and mental disabilities increase caregiver burden (*2*, *3*). Human tau isoforms include three-repeat tau (3R-tau) and four-repeat tau (4R-tau) dependent of the number of a microtubule-binding repeat domain. Alzheimer's disease (AD) brains present both 3R-tau and 4R-tau aggregation with amyloid-β deposits. While amyloid-β enhances tau pathology in AD brains, pathological findings of PSP lack amyloid-β deposits and characterized by the predominance of 4R-tau aggregation in neurons, oligodendrocytes, and astrocytes, which are referred as globose-type neurofibrillary tangles (NFTs), coiled bodies, and tufted astrocytes (TAs), respectively. In particular, TA is the pathologically diagnostic hallmark for PSP (*4*).

The pathogenic mechanism underlying PSP largely remain elusive, but we have reported that the interactions between RNA binding proteins, fused in sarcoma (FUS) and splicing factor proline and glutamine rich (SFPQ), regulate the balance of 3R-tau and 4R-tau expression at the RNA levels, and their functional disturbance is linked to the pathogenesis of tauopathies including PSP (*5*, *6*). However, the mechanism that drives the aggregation of tau protein has not been clearly explained, and genetic animal models that fully phenocopy PSP are not available. Some familial PSP cases harbor pathogenic mutations in the *MAPT*, the gene coding for tau, that promotes tau aggregation (*7*, *8*), while other familial cases and most sporadic cases do not, and their genetic backgrounds that drive aggregation of the nonmutated tau remain unknown.

This study clinically, neuropathologically, and genetically assessed familial and sporadic PSP cases without tau mutations. Our proteomics and genomics analyses revealed genetic variation of filamin-A (*FLNA*) and the protein abundance of FLNA in the PSP brains. We also investigated the role of FLNA in tau aggregation by

[1]Department of Neurology, Nagoya University Graduate School of Medicine, Nagoya, Japan. [2]Department of Neurology, Japanese Red Cross Aichi Medical Center Nagoya Daini Hospital, Nagoya, Japan. [3]Department of Neurology , National Hospital Organization Suzuka National Hospital, Suzuka, Japan. [4]Department of Human Genetics, Yokohama City University Graduate School of Medicine, Yokohama, Japan. [5]Department of Neuropathology, Institute for Medical Science of Aging, Aichi Medical University, Nagakute, Japan. [6]Department of Anatomy and Cell Biology, Nagoya University Graduate School of Medicine, Nagoya, Japan. [7]Department of Molecular Genetics, Brain Research Institute, Niigata University, Niigata, Japan. [8]Research Division of Dementia and Neurodegenerative Disease, Nagoya University Graduate School of Medicine, Nagoya, Japan. [9]Department of Clinical Research Education, Nagoya University Graduate School of Medicine, Nagoya, Japan. [10]Clinical Genetics Department, Yokohama City University Hospital, Yokohama, Japan. [11]Department of Genomic Function and Diversity, Medical Research Institute Tokyo Medical and Dental University, Tokyo, Japan. [12]Section of Viral Vector Development, National Institute for Physiological Sciences, Okazaki, Japan. [13]Department of Functional Brain Imaging, National Institutes for Quantum and Radiological Science and Technology, Chiba, Japan. [14]Department of Psychiatry, Nagoya University Graduate School of Medicine, Nagoya, Japan. [15]Department of Pathology, Brain Research Institute, Niigata University, Niigata, Japan. [16]Department of Neurology and Neuropathology (The Brain Bank for Aging Research), Tokyo Metropolitan Geriatric Hospital and Institute of Gerontology, Tokyo, Japan. [17]Department of Neuropathology, Graduate School of Medicine, The University of Tokyo, Tokyo, Japan.
*Corresponding author. Email: ka2no@med.nagoya-u.ac.jp
†The full membership of the investigators is found at https://humandbs.biosciencedbc.jp/en/hum0043-j-adni-authors for J-ADNI.
‡The full membership of the investigators is found at https://dropbox.com/s/hno4ugftczajwrw/JALPAC%20Investigator%20List.pdf?dl=0 for JALPAC.

analyzing the patient-derived cultured cells and by the newly generated transgenic mice carrying human *FLNA* gene.

RESULTS

Proteomics approaches identified FLNA protein abundance in PSP brains

To investigate molecular mechanisms underlying tau aggregation in PSP, we first performed SDS–polyacrylamide gel electrophoresis (SDS-PAGE) on sarkosyl-insoluble fractions of the PSP patients' and normal control brains and identified specific >250-kDa band in PSP (Fig. 1A). The liquid chromatography–tandem mass spectrometry (LC-MS/MS) analysis for the band determined several proteins including FLNA (table S1). Immunoblotting of the lysates from postmortem brains with various types of neuropathology, including 11 cases with PSP, 10 with corticobasal degeneration (CBD), 10 with AD, six with Parkinson's disease (PD), five with dementia with Lewy bodies (DLB), and five normal control subjects (table S2), demonstrated increases in sarkosyl-insoluble FLNA in PSP (Fig. 1, B to D). Next, we performed immunohistochemistry of the frontal cortex of PSP brains and found that the PSP-specific TAs were immunoreactive to a monoclonal antibody for FLNA (Fig. 1E). Immunofluorescence showed that FLNA was colocalized with the NFTs, coiled bodies, and TAs (Fig. 1F and fig. S1). The tau inclusions in other tauopathies

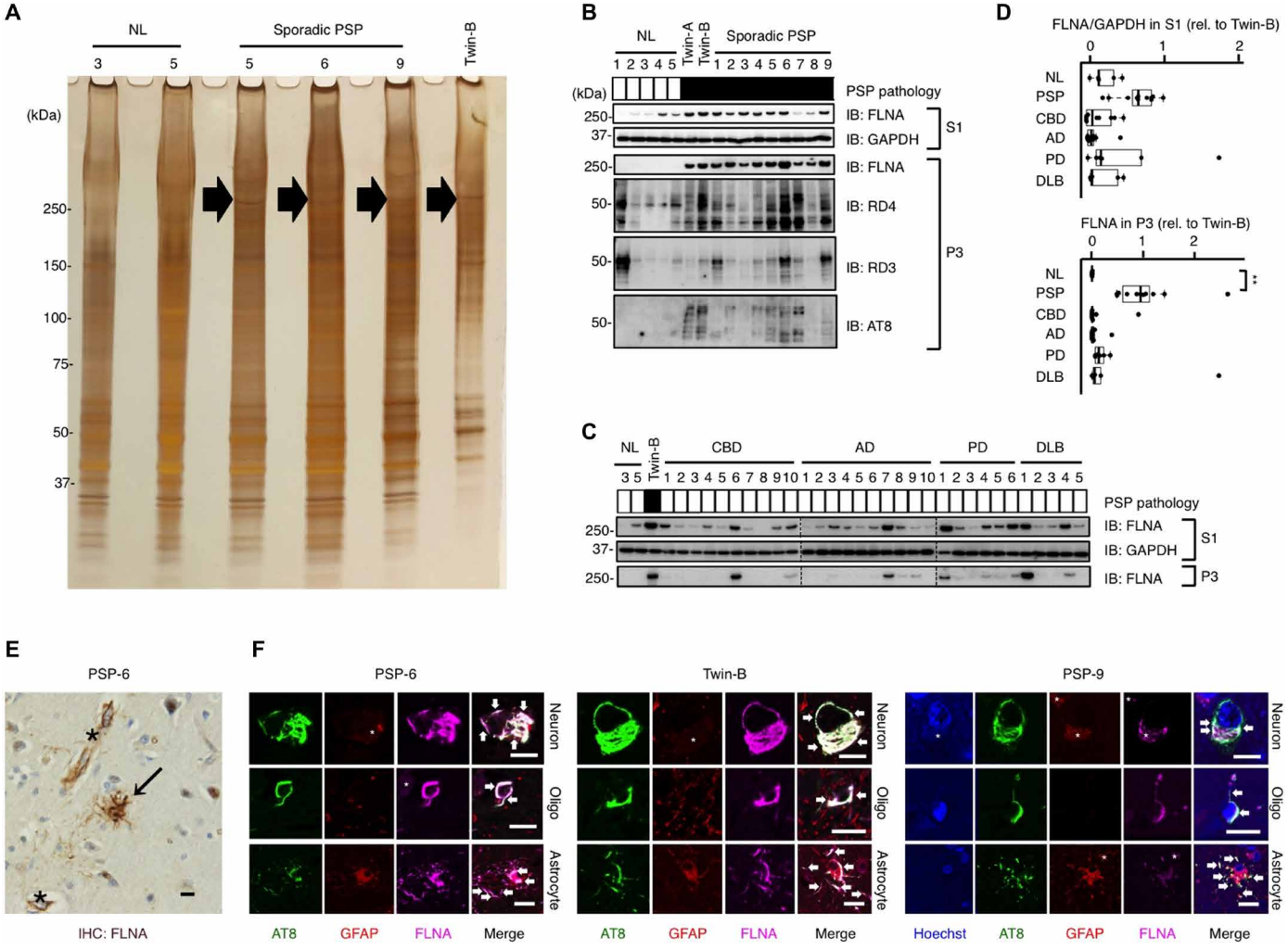

Fig. 1. FLNA protein is abundant in the affected neurons and glial cells of PSP brains. (**A**) Silver-stained SDS-PAGE gel from sarkosyl-insoluble fractions (P3) of the brains from four cases with PSP (PSP-5, PSP-6, PSP-9, and Twin-B) and two normal control subjects (NL-3 and NL-5). Arrows point to the >250-kDa protein bands specific for PSP and those in PSP-6, PSP-9, and Twin-B excised for nanoLC-MS/MS analyses. (**B** and **C**) Immunoblotting (IB) for TBS-extractable fractions (S1) and P3 of the human brains with anti-FLNA antibody. Subjects in (B) include 11 cases with PSP and 5 normal control subjects. Subjects in (C) include 2 normal control subjects (NL-3 and NL-5), Twin-B, 10 with CBD, 10 with AD, 6 with PD, and 5 with DLB. RD4 and RD3 are 4R-tau and 3R-tau isoform–specific antibodies, respectively, and AT8 is a phosphorylated tau antibody. Glyceraldehyde-3-phosphate dehydrogenase (GAPDH) serves as a loading control. Dashed line indicates boundary line between different membranes. (**D**) Box plots show quantitative comparisons for FLNA to GAPDH ratio in S1 and for FLNA levels in P3. All values are relative to Twin-B. (**E**) Immunohistochemistry (IHC) for the frontal cortex of PSP-6 shows that the monoclonal anti-FLNA antibody stains TAs (arrow) and the blood vessels (asterisks). Scale bar, 5 μm. (**F**) Immunofluorescence for the frontal lobes of PSP-6, Twin-B and PSP-9 with anti-FLNA antibody (magenta) and AT8 (green) show colocalization of FLNA and phosphorylated tau in the neurons, oligodendrocytes (oligos), and astrocytes. Anti–glial fibrillary acidic protein (GFAP) antibody (red) was used to identify astrocytes. Arrows show colocalization of AT8 and FLNA. Coarse granular signals (*) indicate autofluorescence of lipofuscin. Scale bars, 10 μm.

including CBD, AD, and Pick's disease (PiD) did not show apparent colocalizations with FLNA (fig. S2). Meanwhile, the findings of no increase in FLNA levels under massive tau induction in tau transgenic mice (fig. S3) suggest that the FLNA lies upstream to the tau pathology.

Genetic analyses identified gene duplications of *FLNA* in the monozygotic twin concordant for PSP

In parallel, we performed whole-exome sequence and chromosome microarray for a Japanese family with monozygotic twin males concordant for tau pathology of PSP (Twin-A and Twin-B) and did not identify any pathogenic variations in the *MAPT* gene but revealed 0.3-Mb recurrent copy number gains at Xq28 including *FLNA* duplications (Fig. 2A and figs. S4 and S5, A to E). The copy number gain was not detected in 513 Japanese healthy control males (fig. S5F). The twins' sister was an asymptomatic heterozygous carrier for the copy number gains and exhibited a skewed X chromosome inactivation (XCI) (fig. S5, C and D). The copy number gain contains 16 annotated protein-coding genes (table S3). The similar copy number gain has been reported in families with X-linked intellectual disability,

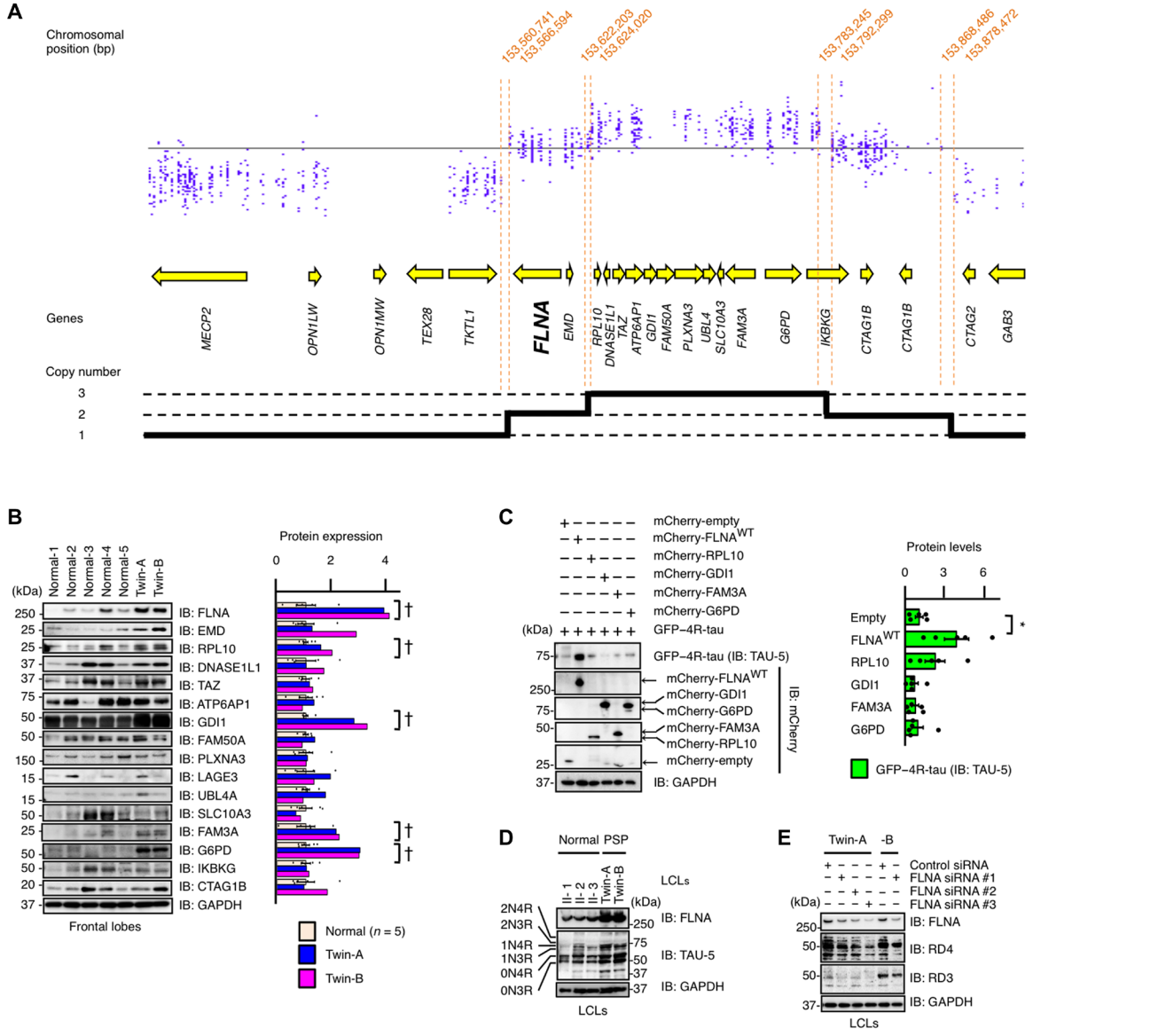

Fig. 2. Gene duplications of *FLNA* are identified in the monozygotic twins with PSP. (**A**) Enlarged view of microarray data of Twin-A. The copy number gain region includes 16 annotated coding genes, and the copy number changes in a stepwise manner at LCRs within the region. The *FLNA* gene is duplicated. bp, base pair. (**B**) Immunoblotting (IB) of the lysates from frontal lobes shows that the levels of proteins coded by 5 (†; *FLNA*, *RPL10*, *GDI1*, *FAM3A*, and *G6PD*) of 16 genes within the copy number gains at Xq28 are higher in the both PSP twins (Twin-A and Twin-B) than the mean + SD of five normal controls. (**C**) IB shows that coexpression of wild-type FLNA (FLNA^{WT}), among the above five proteins, with GFP–4R-tau in HEK293 cells causes significantly higher protein levels of GFP–4R-tau compared to empty ($n = 5$). (**D**) IB of the LCLs using total tau antibody TAU-5 shows higher levels of endogenous FLNA and tau in the PSP twins than their siblings (II-1 to II-3). (**E**) IB of the LCLs from the PSP twins using isoform-specific tau antibodies RD4 and RD3 shows that knockdown of *FLNA* with siRNAs reduces both 4R-tau and 3R-tau concentrations. Values are presented as means ± SEM. *$P < 0.05$. Statistics obtained from one-way ANOVA with Tukey-Kramer tests in (C).

but the protein expression levels of each gene in their brains were unanalyzed (*9*). Immunoblotting for the frontal lobes of the twins found a high expression of FLNA, ribosomal protein L10 (RPL10), guanosine diphosphate dissociation inhibitor 1 (GDI1), family with sequence similarity 3 member A (FAM3A), and glucose-6-phosphate dehydrogenase (G6PD) among the 16 proteins in both twins compared to normal control subjects (Fig. 2B). To examine the contribution of these five proteins to 4R-tau pathogenesis, the mCherry-tagged vector constructs for each gene and the green fluorescent protein (GFP)–tagged wild-type 4R-tau (GFP–4R-tau) vector constructs were cotransfected into human embryonic kidney (HEK) 293 cells. We found that FLNA, but not the other four proteins, increased the protein level of GFP–4R-tau (Fig. 2C) and also the GFP–3R-tau level (fig. S6A). In the lymphoblast cell lines (LCLs) of the twins, both endogenous FLNA and tau levels were higher than those of their healthy siblings (Fig. 2D). In addition, small interfering RNA (siRNA)–mediated knockdown of FLNA corrected the aberrant levels of endogenous tau in the LCLs. The treatments of FLNA siRNAs inhibited endogenous 4R-tau and 3R-tau levels in the LCLs of the twins (Fig. 2E). RPL10 overexpression also showed a trend of increasing GFP–4R-tau levels in HEK293 cells (Fig. 2C), but RPL10 knockdown had no effect on the tau levels in the LCLs (fig. S6B).

Rare variants of *FLNA* are associated with PSP

To investigate the involvement of the *FLNA* gene in sporadic PSP, we extended the mutational and structural analyses using a Japanese dataset consisting of 312 cases with PSP, 71 cases with CBD, 141 cases with AD, and 499 controls (table S4). We did not detect the copy number gains at Xq28 including *FLNA* duplications in the groups. Twelve cases with PSP had rare variants (minor allele frequency < 1%) of *FLNA* gene, including six missense variants (p.Ser2523Asn, p.Arg2334Cys, p.Val2191Met, p.Ala2075Ser, p.Arg2003His, and p.Leu1980Val) and one splicing variant (c.4755 + 5G > A).Two cases with CBD also had the p.Ser2523Asn missense variant. Three cases with AD had a different missense variant from PSP and CBD (p.Thr2101Met). Five controls had three missense variants (p.Tyr2106Cys, p.Asp2074Asn, and p.Tyr2642Cys) and one splicing variant (c.4755 + 5G > A) (Table 1 and table S5). An association study for each tauopathy and *FLNA* rare variant showed that PSP had the highest rate compared to controls (odds ratio for PSP, 3.91; 95% confidence interval, 1.27 to 14.27; Table 2).

FLNA enhances phosphorylation, protein stability, and sarkosyl insolubility of 4R-tau

Immunoblotting using the two major antibodies for phosphorylated tau, AT8 and PHF-1, showed that FLNA induced a hyperphosphorylation of GFP–4R-tau in HEK293 cells (Fig. 3A). To examine the effects of FLNA on the protein stability of 4R-tau, we performed a cycloheximide (CHX) chase assay by coexpressing GFP–4R-tau and FLNA in HEK293 cells. When coexpressed with FLNA, GFP–4R-tau had a longer half-life compared with that without FLNA coexpression (Fig. 3B). These findings indicate that FLNA augments 4R-tau protein levels by increasing tau phosphorylation and protein stability. We next extracted the tris-buffered saline (TBS)–extractable and sarkosyl-insoluble fractions of HEK293 cells coexpressing GFP–4R-tau and varying amounts of FLNA. In whole homogenates, the protein levels of GFP–4R-tau increased proportionally along with the amount of cotransfected FLNA (Fig. 3C). Notably, the highest induction of FLNA resulted in smeared bands of GFP–4R-tau in the whole homogenates and a significantly higher expression of GFP–4R-tau in both the TBS-extractable and sarkosyl-insoluble fractions on gels, indicative of GFP–4R-tau aggregation. In this context, the protein interaction between GFP–4R-tau and FLNA was confirmed by a co-immunoprecipitation using an antibody against tau, TAU-5, in the homogenates (Fig. 3D). We also found that FLNA augmented the interaction of GFP–4R-tau with heat shock protein 90 (HSP90), HSP70, HSP40, and ubiquitin. These results indicated that the abundance of FLNA protein provokes its interaction with 4R-tau, which results in a heat shock response and ubiquitination against the 4R-tau aggregates. In addition, immunocytochemical assay using rat primary astrocytes coexpressing

Table 1. Rare variants of *FLNA* identified in PSP, CBD, AD, and control. PSP, progressive supranuclear palsy; CBD, corticobasal degeneration; AD, Alzheimer's disease; n/a, not assessment.

Variant		PSP (*N* = 312)	CBD (*N* = 71)	AD (*N* = 140)	Control (*N* = 499)	Allele frequency in public databases				CADD
Codon change	Amino acid change					ExAC	gnomAD	HGVD	ToMMo	
c.7568G > A	p.Ser2523Asn	3	2	0	0	0.0004	0.0004	0.0025	0.0022	17.2
c.7000C > T	p.Arg2334Cys	1	0	0	0	1.23×10^{-5}	1.66×10^{-5}	n/a	0.0006	23.3
c.6571G > A	p.Val2191Met	1	0	0	0	2.31×10^{-5}	5.50×10^{-5}	n/a	n/a	19.1
c.6223G > T	p.Ala2075Ser	1	0	0	0	n/a	n/a	n/a	n/a	24.3
c.6008G > A	p.Arg2003His	1	0	0	0	n/a	n/a	n/a	n/a	24.9
c.5938C > G	p.Leu1980Val	1	0	0	0	n/a	n/a	n/a	n/a	21.0
c.4755 + 5G > A	-	4	0	2	2	6.26×10^{-5}	5.67×10^{-5}	0.0016	0.0039	22.5
c.6302C > T	p.Thr2101Met	0	0	3	0	n/a	n/a	0.0009	0.0008	26.8
c.6317A > G	p.Tyr2106Cys	0	0	0	1	n/a	n/a	n/a	n/a	27.0
c.6220G > A	p.Asp2074Asn	0	0	0	1	3.49×10^{-5}	2.82×10^{-5}	n/a	0.0003	13.7
c.7925A > G	p.Tyr2642Cys	0	0	0	1	3.46×10^{-5}	n/a	n/a	1.00×10^{-4}	28.8

Table 2. Association between *FLNA* rare variant and tauopathies. CI, confidence interval.

Cohort	Allele frequency – no./ total no. (%)	Odds ratio (95% CI)
PSP (*N* = 312)	12/440 (2.73)	3.91 (1.27–14.27)
CBD (N = 71)	2/107 (1.87)	2.65 (0.25–16.47)
AD (*N* = 140)	5/221 (2.26)	3.23 (0.74–14.16)
Control (*N* = 499)	5/703 (0.71)	-

GFP–4R-tau and FLNA showed that hyperphosphorylated GFP–4R-tau aggregates were localized within the proximal portions of processes and cell bodies, reminiscent of TAs in PSP (Fig. 3E), and immunoblotting showed that FLNA substantially increased GFP–4R-tau levels (Fig. 3F).

The missense variants of FLNA alter its binding to F-actin and subsequently change protein levels of 4R-tau

The microtubule-binding repeat domains of tau contain multiple interaction sites with F-actin (*10*). FLNA has an actin-binding domain (ABD) at the N terminus and promotes orthogonal branching of F-actin (*11*). The mutant FLNA with p.Ala39Gly in the ABD loses the ability of F-actin binding (fig. S7A) (*12*). Immunoblotting showed that the p.Ala39Gly mutant FLNA led to reduce F-actin polymerization and induction of GFP–4R-tau in HEK293 cells compared with the wild-type FLNA (fig. S7, B and C). On the basis of the mutational analysis for the Japanese PSP and CBD cohorts, we found five cases of an amino acid substitution at Ser^{2523}, the residue at which phosphorylation can occur and decrease FLNA binding to F-actin (*13*, *14*). Immunoblotting of lysates from HEK293 cells using an antibody for phosphoserine-2523 confirmed that the Ser^{2523}Asn substitution attenuated phosphorylation at the Ser^{2523} (fig. S7D) and enhanced insolubility of GFP–4R-tau at higher levels compared to the wild-type FLNA (fig. S7E). The nonphosphorylated variant of FLNA with p.Ser2523Ala also substantially enhanced insolubility of GFP–4R-tau, suggesting that dephosphorylated state at Ser2523 can drive tau aggregation (fig. S7E). Furthermore, we found that the six PSP-associated missense rare variants (p.Ser2523Asn, p.Arg2334Cys, p.Val2191Met, p.Ala2075Ser, p.Arg2003His, and p.Leu1980Val) induced F-actin polymerization (fig. S7F), and some of them tended to increase GFP–4R-tau levels compared to the wild-type FLNA (fig. S7G).

In vivo overexpression of FLNA develops gray matter heterotopia and enhances protein levels of 4R-tau through interaction with F-actin

We next applied in utero electroporation (IUE) of cytomegalovirus (CMV) enhancer/chicken β-actin (CAG) promoter plasmids of FLNA and GFP–4R-tau to the mouse brain at an embryonic day 14 (E14). The analysis of E18 brain showed that the wild-type FLNA caused developmental abnormalities of neural migration defects and gray matter heterotopia (Fig. 4A and fig. S8A). The electroporated cells in the heterotopia were negative for Sox2, a neural progenitor cell marker (*15*), and instead immunopositive for Satb2, an upper cortical layer marker (*16*), supporting the finding of the migration defects (fig. S8B). The protein levels of GFP–4R-tau were enhanced by wild-type FLNA, but not by p.Ala39Gly mutant FLNA that abrogates the binding ability to F-actin (Fig. 4A). Phalloidin staining indicated that the wild-type FLNA promoted F-actin polymerization in the neurons expressing GFP–4R-tau (fig. S8C). To visualize F-actin dynamics in neurons overexpressing FLNA, we performed IUE with the plasmids of FLNA and lifeact, an actin-binding peptide that stains F-actin structures in living cells, and found that overexpression of FLNA induced a slowdown of actin dynamics with F-actin accumulation (movie S1). Primary cortical neurons from the E15 fetuses showed that the wild-type FLNA caused AT8 hyperphosphorylation of GFP–4R-tau with F-actin accumulation, which was compromised by the treatment with an actin depolymerizer cytochalasin D (Fig. 4B). These results indicate that FLNA increases GFP–4R-tau levels through direct interaction mediated by F-actin. We also analyzed the postnatal day 7 (P7) brains coexpressing wild-type FLNA and GFP–4R-tau by E14 IUE and found abnormal accumulation of GFP–4R-tau in neurons, oligodendrocytes, and astrocytes (Fig. 4C and fig. S8, D to E). In addition, immunoblotting and quantitative real-time polymerase chain reaction (qRT-PCR) demonstrated that FLNA increased the protein levels but not the RNA levels of GFP–4R-tau, which would in turn promote 4R-tau aggregation (Fig. 4D and fig. S8F).

Viral induction of the truncated human FLNA enhances murine and human tau in adult mouse brains

To induce overexpression of FLNA in the adult murine brains, we used an adeno-associated virus (AAV) vector–mediated approach. Because the size of full-length human *FLNA* cDNA is too large to be packaged into virions, we designed AAVs expressing the truncated versions of FLNA that contains essential domains for the interaction with tau. FLNA has N-terminal ABD and 24 immunoglobulin (Ig)–like internally homologous repeats (Ig1-24). The last C-terminal Ig repeat (Ig24) serves as a dimerization domain. We found that Ig9-15 region promoted F-actin polymerization and increased protein levels of GFP–4R-tau in HEK293 cells more effectively compared to Ig1-9 or Ig16-23 region (fig. S9, A to E), thus prepared AAV vectors expressing the truncated FLNA consisting of ABD, Ig9-15, and Ig24 (ΔFLNA) under the control of a chicken β-actin promoter (Fig. 5A). Co-immunoprecipitation assay for the lysates from both ΔFLNA and GFP–4R-tau–transduced HEK293 cells showed the protein-protein interactions between ΔFLNA and GFP–4R-tau (Fig. 5B). Adult wild-type C57BL/6 mice exclusively express a 4R isoform for tau (*17*). We performed stereotaxic injections of AAV-expressing ΔFLNA, which promoted F-actin polymerization (fig. S10), into the frontal cortex of 2-month-old wild-type C57BL/6 mice and found increased endogenous 4R-tau and AT8-immunopositive phosphorylated tau levels in the neurons at 3 months old (Fig. 5, C to E). Similarly, we evaluated the effect of ΔFLNA on human tau in transgenic mice that harbor human *MAPT* gene in the absence of mouse *Mapt* gene (TAU KO; hT-PAC-N), which express both human 4R-tau and 3R-tau isoforms (*17*). Immunohistochemistry of the brains showed enhanced human 4R-tau and 3R-tau expression in the ΔFLNA-transduced neurons, and immunoblotting showed correspondingly increased protein levels of human 4R-tau and 3R-tau in both TBS-extractable and sarkosyl-insoluble fractions (Fig. 5, F and G), suggesting no preference for tau isoform as FLNA substrate.

Transgenic mice carrying full-length human FLNA showed hyperphosphorylated 4R-tau in neurons and glial cells

Our findings that FLNA drives tau aggregation further led us to generate transgenic mice expressing full-length human FLNA (FLNA-Tg)

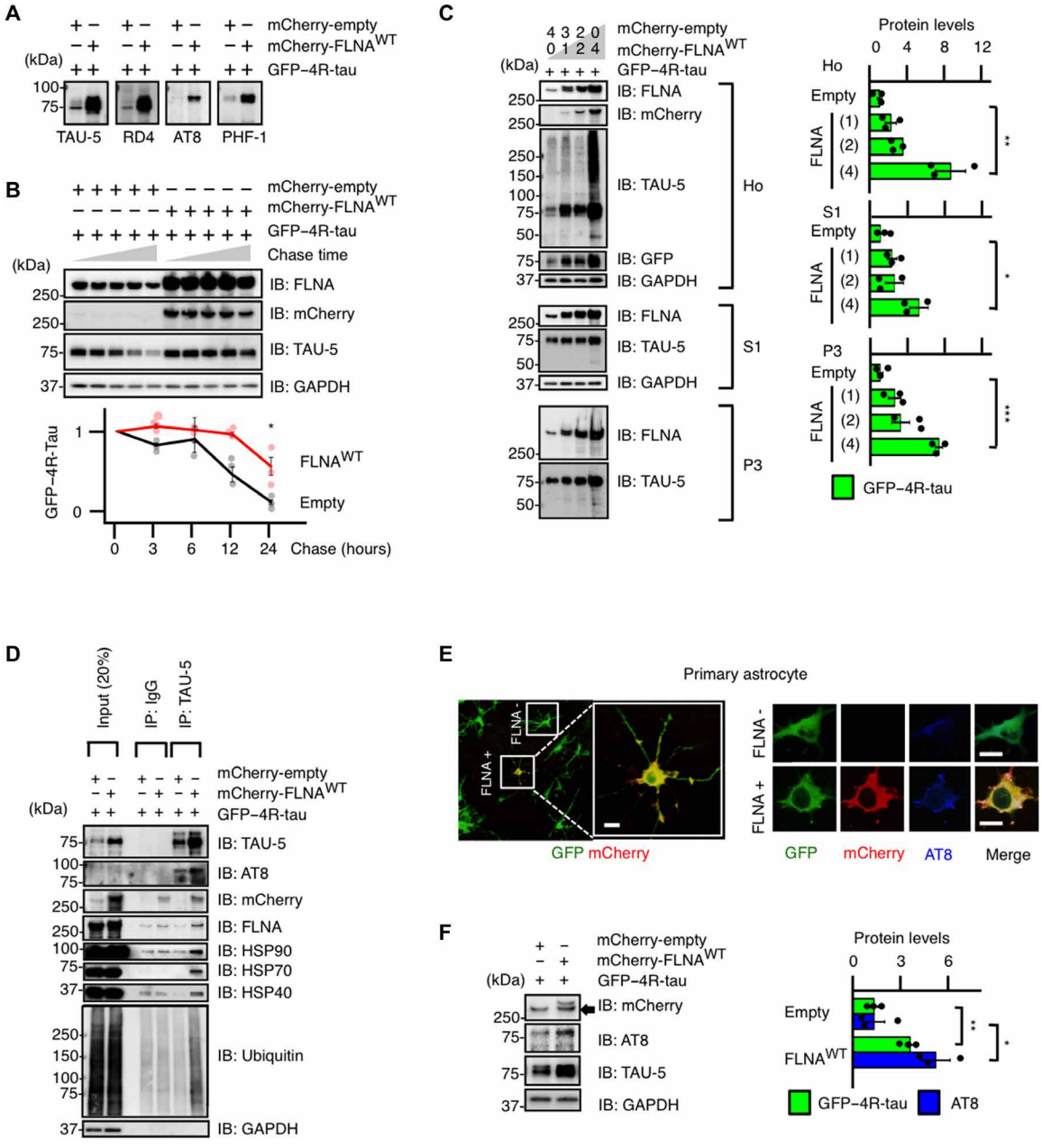

Fig. 3. FLNA enhances the phosphorylation, protein stability and sarkosyl-insolubility of tau. (**A**) Immunoblotting (IB) of the lysates from HEK293 cells shows FLNA^{WT} induces phosphorylation of GFP–4R-tau at the epitopes recognized by the two phosphorylated tau antibodies AT8 (Ser^{202}/Thr^{205}) and PHF-1 (Ser^{396}/Ser^{404}). (**B**) IB of the lysates from CHX chase assay in HEK293 cells shows that the GFP–4R-tau protein levels at 24 hours are significantly higher when FLNA are coexpressed compared to empty ($n = 3$). The levels of GFP–4R-tau are normalized to those of GAPDH at 0 hour. (**C**) IB of the lysates from HEK293 cells shows that overexpression of FLNA^{WT} in HEK293 cells increases GFP–4R-tau concentration in homogenates (Ho), S1, and P3 ($n = 3$). (**D**) Immunoprecipitation (IP) assay. More FLNA^{WT} proteins are coimmunoprecipitated with TAU-5 from lysates of HEK293 coexpressing GFP–4R-tau and FLNA. More HSP90, HSP70, HSP40, and ubiquitin are also coimmunoprecipitated. (**E**) Immunofluorescence shows AT8-immunopositive tau aggregates (blue) in the astrocytes coexpressing GFP–4R-tau (green) and mCherry-tagged FLNA (red) (FLNA+) but not in the astrocytes expressing sole GFP–4R-tau (FLNA–). (**F**) IB of homogenates from the astrocytes shows that FLNA^{WT} significantly increases the protein levels of GFP–4R-tau with AT8-immunopositive hyperphosphorylation ($n = 3$). Arrow indicates nonspecific band. Scale bars, 10 μm. Values are presented as means ± SEM. ***$P < 0.001$, **$P < 0.01$, and *$P < 0.05$. Statistics obtained from Tukey-Kramer tests in (C) and Student's t tests in (F).

under the CAG promoter. Immunohistochemistry of the brains of the 5-month-old FLNA-Tg mice showed overexpression of FLNA in the brains, especially in the neurons of the deeper cortical layer and hippocampal CA1 region (Fig. 6A). FLNA was also expressed partly in the astrocytes and oligodendrocytes, but their expression levels were mild (Fig. 6A). Of note, murine endogenous 4R-tau deposits were found in the neurons of the cerebral cortex and hippocampus (Fig. 6B). A few AT8-immunopositive neurons appeared in frontal cortex and midbrain but did not appear in hippocampus (fig. S11). AT8-immunopositive glial cells were also observed in the

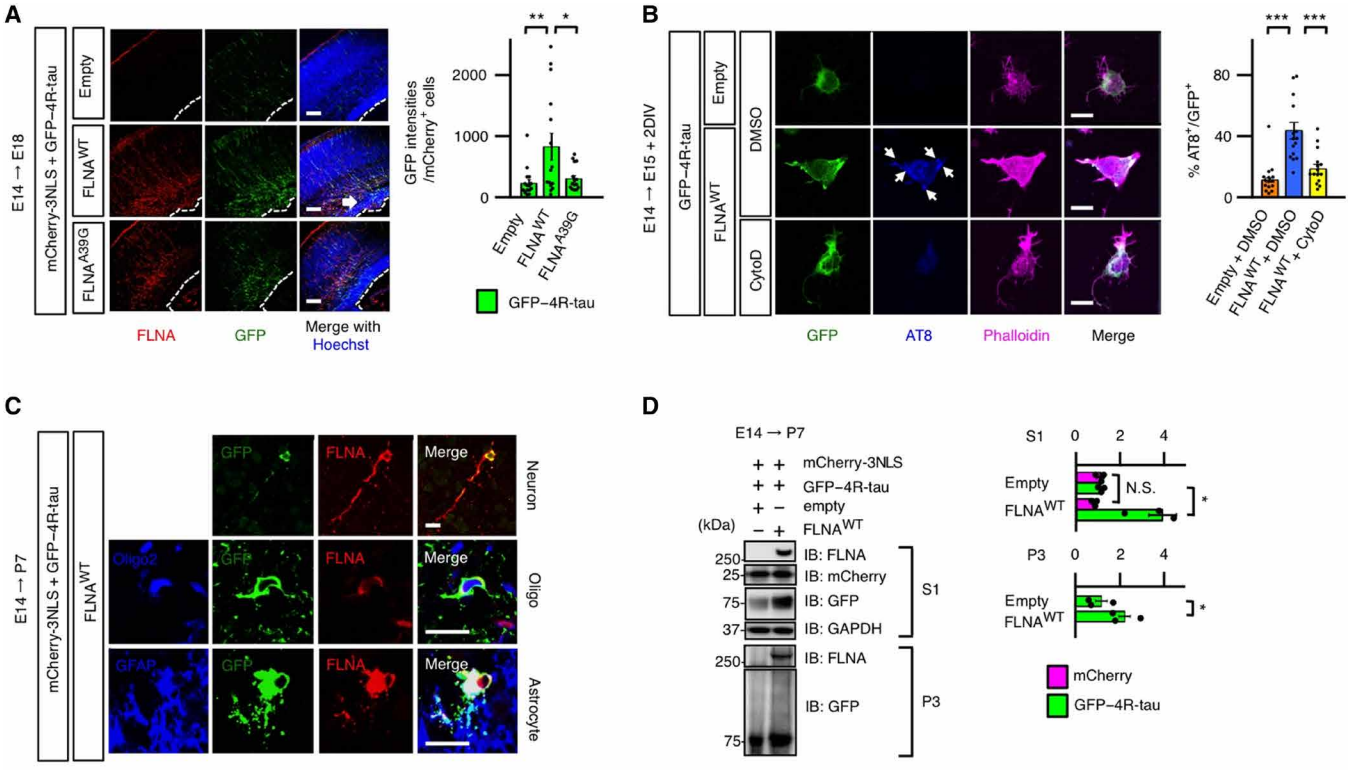

Fig. 4. Induction of human FLNA by electroporation enhances GFP–4R-tau protein levels through F-actin in murine brains. (**A**) Immunofluorescence for the E18 mouse brains that were electroporated with the indicated plasmids at E14 ($n = 15$). The electroporation of FLNA^{WT} (red), but not mutant FLNA (FLNA^{Ala39Gly}) that abrogates the binding ability to F-actin, results in heterotopia (arrow) and a higher immunoreactivity for GFP–4R-tau (green) compared to empty. The immunoreactivity is normalized to the count of the mCherry-labeled electroporated cells. Scale bars, 100 μm. (**B**) Immunofluorescence for primary cortical neurons from E15 brain that were electroporated with the indicated plasmids at E14, followed by the treatment of 0.1% dimethyl sulfoxide (DMSO) or 20 nM cytochalasin D (CytoD) ($n = 15$). Overexpression of FLNA^{WT} (red) with DMSO shows AT8-immunopositive tau aggregates (arrows) and significantly higher area ratio of AT8 (blue) to GFP (green) (% AT8/GFP) on 2 days in vitro (DIV) compared to empty; this phenomenon was attenuated with CytoD treatment. Phalloidin stain (magenta) was used to identify F-actin. Scale bars, 10 μm. (**C**) Immunofluorescences for the P7 brains that were electroporated with the indicated plasmids at E14. The neurons, oligodendrocytes, and astrocytes in the P7 brains show accumulations of GFP–4R-tau (green) with FLNA^{WT} (red). Anti-GFAP antibody (blue) was used to identify astrocytes. Scale bars, 10 μm. (**D**) Immunoblotting (IB) of lysates from the P7 brains with the IUE shows that FLNA^{WT} significantly increases the protein levels of GFP–4R-tau compared to empty in S1 and P3 ($n = 3$). Values are presented as means ± SEM. N.S., not significant. ***$P < 0.001$, **$P < 0.01$, and *$P < 0.05$. Statistics obtained from Tukey-Kramer tests in (A) and (B) and Student's t tests in (D).

midbrain and hypothalamus. Coaggregation of AT8-immunopositive phosphorylated 4R-tau and FLNA was found in the neurons (Fig. 6C) and only moderately in the oligodendrocytes and astrocytes (fig. S12). Immunoblotting of the frontal cortex extracts from the 5-month-old FLNA-Tg mice showed increased endogenous 4R-tau and augmented sarkosyl-insoluble AT8-immunoreactive phosphorylated 4R-tau (Fig. 6D). Last, primary cortical neurons from the forebrains of E15 FLNA-Tg mice showed AT8-immunopositive 4R-tau phosphorylation and defective neurite outgrowth at 6 days in vitro, which were rescued by lentiviral short hairpin RNA–mediated knockdown of FLNA (Fig. 6E). These observations demonstrate that induction of FLNA drives tau aggregation in vivo.

DISCUSSION

In this study, we demonstrated that autopsied PSP brains show enriched FLNA in tau pathological lesions and that the experimental increases in FLNA leads tau aggregation through their interactions with F-actin. Moreover, we found that some cases with PSP carried structural or single-nucleotide variations on the *FLNA* gene. Namely, gene duplications of *FLNA* were identified in the monozygotic twins with the neuropathological concordance of PSP, and results of rare variant association analysis for Japanese sporadic PSP cohorts provided the possibility of *FLNA* as a genetic contributing factor of PSP. To our knowledge, there is no previous studies showing the genetic involvement of *FLNA* in PSP and other tauopathies, but some pathological investigations of the AD brains have identified a colocalization of FLNA with tau in NFTs (*18*, *19*). Our study extended this finding to 4R-tau inclusion in PSP such as NFTs, coiled bodies, and TAs. Although massive tau was found not to induce the recruitment FLNA in the brains of the rTg4510 mice carrying human *MAPT* gene that encodes tau, the FLNA-Tg mice successfully induced endogenous tau aggregation in the brains without the presence of mutant tau, presenilin-1, or amyloid-β precursor protein, the known driver of the aggregation (*20*, *21*). Furthermore, the findings of reversal of FLNA-driven accumulations in the neurons by inhibiting FLNA expression helps to support the notion that FLNA can act upstream of tau.

FLNA is an actin-binding protein that regulates actin polymerization and neuronal migration in the cerebral cortex (*22*, *23*). Loss-of-function mutations in *FLNA* are known to cause X-linked periventricular nodular heterotopia (*23*, *24*), whereas a prior study showed

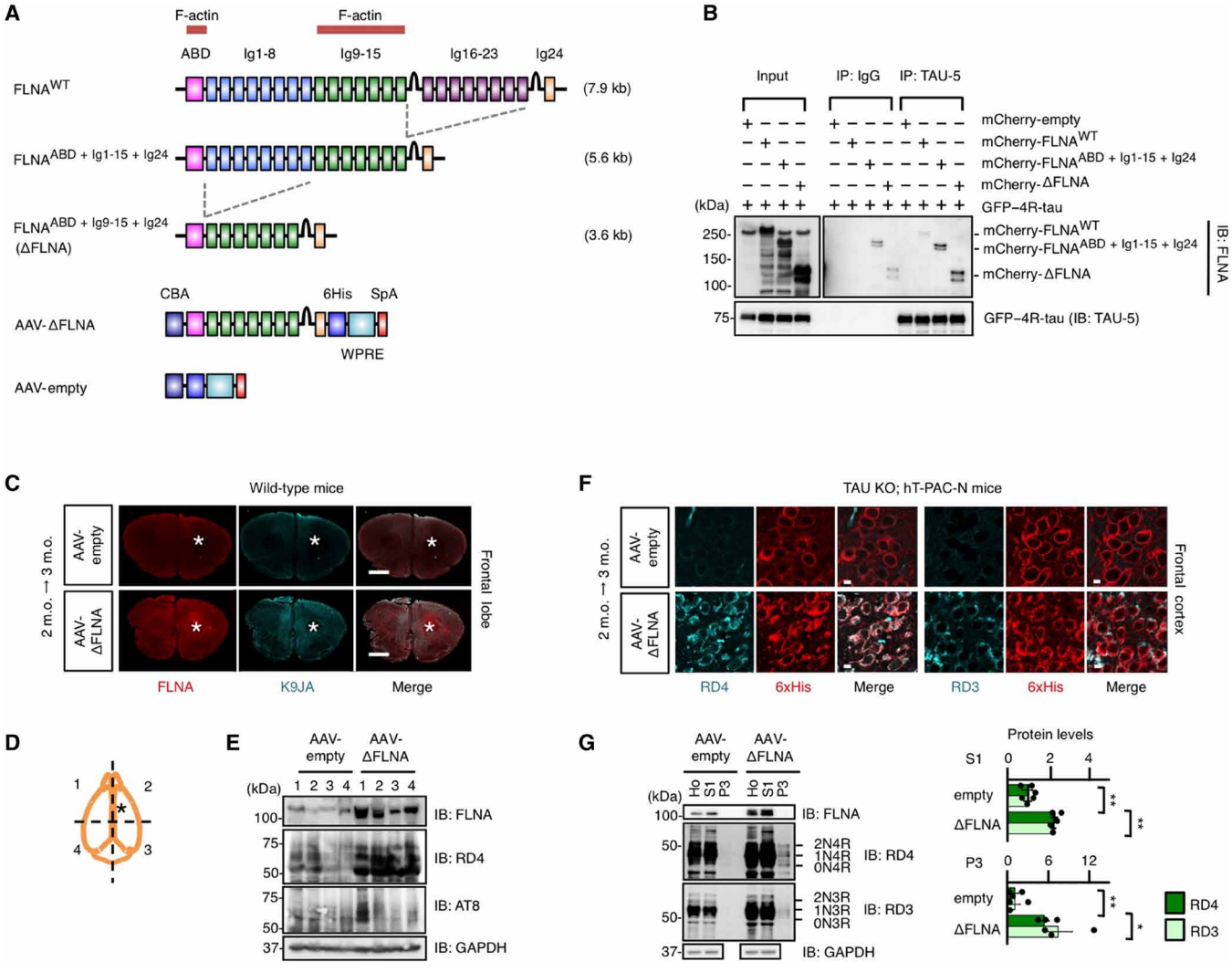

Fig. 5. Stereotaxic injections of AAV-ΔFLNA enhance murine and human tau protein levels in vivo. (**A**) Structures of full-length FLNA (FLNA^{WT}) and two shortened FLNA; FLNA$^{ABD + Ig1\text{-}15 + Ig24}$ and FLNA$^{ABD + Ig9\text{-}15 + Ig24}$ (ΔFLNA). FLNA has N-terminal actin-binding domain (ABD) and 24 immunoglobulin-like internally homologous repeats (Ig1-24). The last C-terminal Ig repeat (Ig24) serves as a dimerization domain. The AAV vectors contain chicken β-actin (CBA) promoter, 6xHis tag, woodchuck hepatitis virus posttranslational regulatory element (WPRE), and SV40 poly(A) signal (SpA). (**B**) Immunoprecipitation (IP) assay and immunoblotting (IB) with antibody TAU-5 for the lysates from HEK293 cells transfected with the indicated constructs. The protein interaction with FLNA and GFP–4R-tau is shown with the transfections of FLNA$^{ABD + Ig1\text{-}15 + Ig24}$ and ΔFLNA. (**C**) Immunofluorescence using anti-FLNA antibody (red) and total tau antibody K9JA (turquoise) for the coronal sections from 3-month-old (m.o.) wild-type C57BL/6 mouse brains that had been injected stereotaxically at 2 months old with AAV-ΔFLNA or AAV-empty. Asterisks indicate the injected sites. Scale bars, 1 mm. (**D**) Schema represents the sampling position (#1 to #4) of the AAV-injected brains for IB. Asterisks indicate the injected sites. (**E**) IB using RD4 and AT8 for homogenates from the AAV-injected brains of the wild-type mice shows that ΔFLNA expression increases protein levels of murine endogenous tau and induces AT8 hyperphosphorylation. (**F**) Immunofluorescence using anti-6xHis tag antibody (red) and isoform-specific tau antibody RD4 or RD3 (turquoise) for coronal sections from the 3-month-old TAU KO; hT-PAC-N mouse brains that injected stereotaxically at 2 months old with AAV-ΔFLNA or AAV-empty. Scale bars, 10 μm. (**G**) IB using RD4 and RD3 for homogenates from the injected brains of the TAU KO; hT-PAC-N mice shows that ΔFLNA expression significantly increases protein levels of human 4R-tau and 3R-tau ($n = 3$). Values are presented as means ± SEM. ***$P < 0.001$, **$P < 0.01$, and *$P < 0.05$. Statistics obtained from Student's t tests in (G).

that overexpression of FLNA by IUE disturbs the neuronal migration in the murine forebrain (*25*). Using similar methods with the plasmids encoding FLNA and GFP–4R-tau, we here showed that FLNA leads to accumulations of GFP–4R-tau and actin polymerization in the neurons and the disturbance of neuronal migration. These pathological changes were not induced by p.Ala39Gly mutant FLNA, which abrogates the F-actin–binding ability, suggesting that FLNA interacts with tau through F-actin. In primary cortical neurons, pharmacological actin depolymerization mitigated the hyperphosphorylation of GFP–4R-tau. Moreover, the injection of AAV-ΔFLNA, the truncated form of FLNA that retains the F-actin–binding ability, even induced the accumulations of endogenous murine tau and transgene-derived human tau in the adult murine brain. Tau has been reported to induce neurodegeneration mediated by extensive polymerization of F-actin (*26*, *27*). Together, our study suggests that FLNA accelerates the F-actin–mediated aberrant interaction with tau and thus drives tau-induced neurodegeneration. In accordance, recent studies have identified genetic variations of

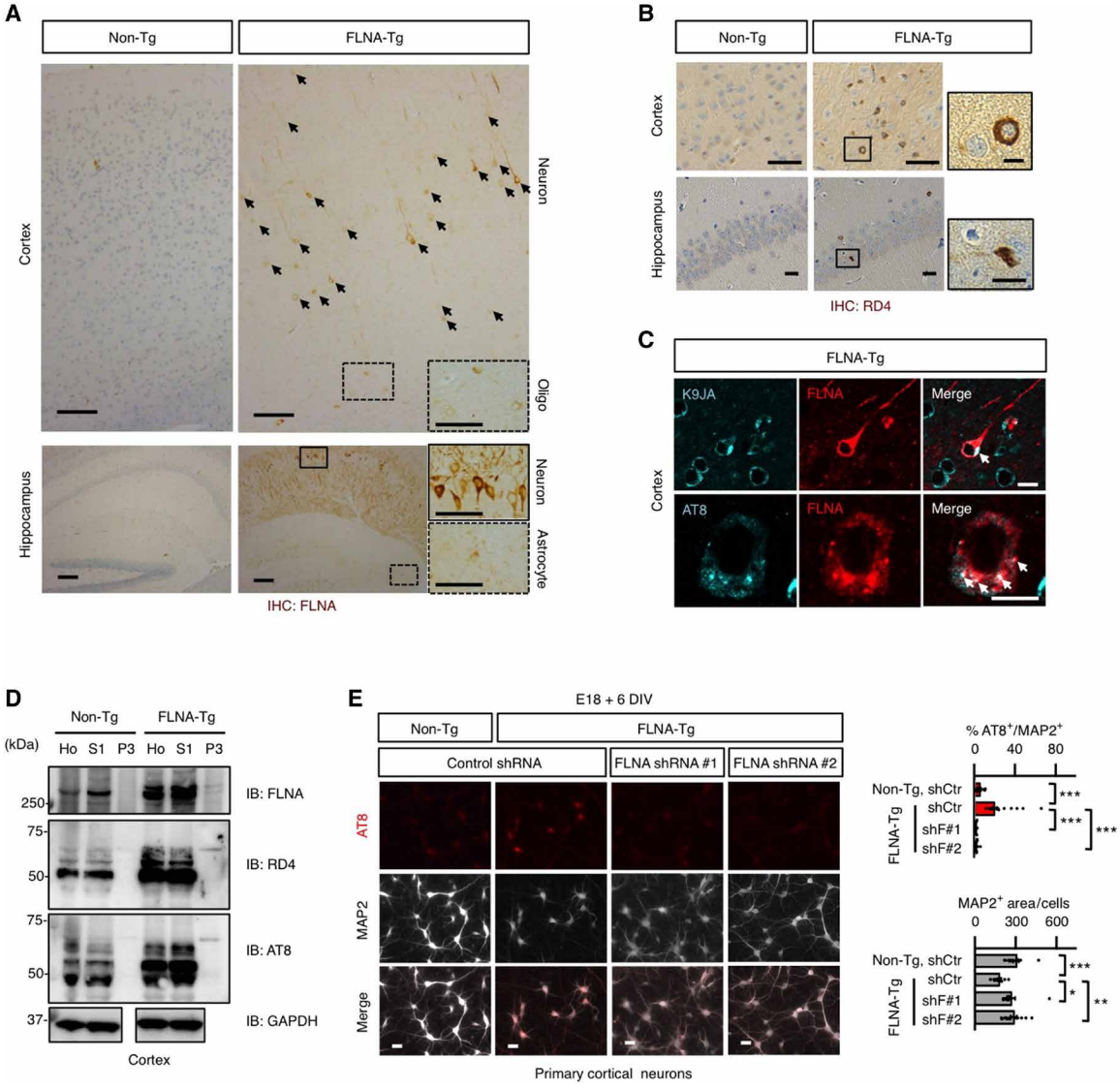

Fig. 6. FLNA transgenic mice exhibit endogenous 4R-tau aggregation in the brains. (**A**) Immunohistochemistry for the brains of 5-month-old FLNA transgenic mice (FLNA-Tg) shows that anti-FLNA antibody stains in the neurons of cerebral cortex and hippocampus, the oligodendrocytes of corpus callosum, and the astrocytes of hippocampus but not in those of nontransgenic littermate controls (non-Tg). Scale bars, 50 μm. (**B**) Immunohistochemistry for the brains of 5-month-old FLNA-Tg shows RD4-immunopositive tau deposits in cerebral cortex and hippocampus. Scale bars, 100 μm (left) and 10 μm in the enlarged images (right). (**C**) Immunofluorescence shows K9JA-immunopositive or AT8-immunopositive tau deposits (turquoise) in the FLNA-stained neurons (red) of FLNA-Tg in the neurons of cortex. Scale bars, 10 μm. (**D**) Immunoblotting (IB) using anti-FLNA antibody, RD4, and AT8 for the frontal lobes from the 5-month-old FLNA-Tg shows sarkosyl-insoluble phosphorylated 4R-tau (arrowhead) and overexpression of FLNA. (**E**) Immunofluorescence for primary cortical neurons of FLNA-Tg show a higher area ratio of AT8 (red) to MAP2 (gray) (%AT8/MAP2) and a lower MAP2 immunoreactivity per cells on 6 DIV compared to those of non-Tg, but the knockdown of *FLNA* with short hairpin RNAs (shRNAs) (shF#1 and shF#2) corrects these findings ($n = 12$). The control shRNA (shCtr) was used for a negative control. The microtubule-associated protein 2 (MAP2) immunoreactivity is normalized to the count of neurons. Scale bars, 50 μm. Values are presented as means ± SEM. ***$P < 0.001$, **$P < 0.01$, and *$P < 0.05$. Statistics obtained from Tukey-Kramer tests in (E).

leucine-rich repeat kinase 2 (*LRRK2*) in PSP (*28*–*30*), and LRRK2 protein has been shown to increase tau-mediated neurotoxicity through excess stabilization of F-actin (*31*).

The monozygotic twins concordant for PSP (Twin-A and Twin-B) shared PSP-tau pathology, including neuronal loss, gliosis, and 4R-tau–positive globose-type NFTs and TAs mainly in the subthalamic nucleus, globus pallidus, substantia nigra, tegmentum of the brainstem, and cerebellar dentate nucleus as well as depigmentation of the substantia nigra. These findings indicate that the neurodegenerative pathologies of the twins are compatible with PSP; however, the brain weight of Twin-A and Twin-B was 970 and 775 g, respectively, being smaller than those of sporadic PSP cases in a previous report (1.1 ± 0.02 kg in 48 PSP cases) (*32*). Moreover, gray matter heterotopia was observed in Twin-B. Because mostly sporadic PSP did not show neurodevelopmental anomalies, the twins' PSP pathologies are not completely consistent with those of sporadic PSP. Even so, the filamin-A protein abundance in 4R-tau inclusions is common between the twins and sporadic PSP and could be an important key for understanding the heterogeneous pathogenesis of PSP.

Among rare variants of *FLNA* identified in PSP, p.Ser2523Asn missense rare variant is located at the known phosphorylated site of FLNA and induced sarkosyl-insoluble GFP–4R-tau and p.Ser2523Ala nonphosphorylated variant. This suggests that FLNA could induce tau aggregation in a dephosphorylated state at Se^{r2523}. p.Ser2523Asn was identified in two cases with CBD in addition to three cases with PSP. All six PSP-associated missense rare variant, including p.Ser2523Asn, induced F-actin polymerization compared to wild-type FLNA. Other PSP-associated missense variants except for p.Ser2523Asn did not apparently augment 4R-tau in the cellular experiments but could contribute to the pathogenesis through interacting with F-actin. Although our association study showed a lower odds ratio in AD than in PSP, the result does not deny the possibility that FLNA contribute to the pathogenesis of AD because three cases with AD shared the p.Thr2101Met missense variant. Further large-scale studies for FLNA rare variant in various tauopathies are needed.

The tau inclusions in PSP brains consist predominantly of 4R-tau. Our pathological analyses for various tauopathies—including PSP, CBD, AD, and PiD—suggested that FLNA-driven 4R-tau aggregation tend to be specific to PSP. FLNA is thus expected to increase 4R-tau levels more effectively than 3R-tau levels through interacting with F-actin, while the injections of AAV-ΔFLNA increased protein levels of both 3R-tau and 4R-tau in the humanized tau mouse brains. It can be speculated that FLNA prefers to bind to 4R-tau since the 4R-tau has structurally additional F-actin–interacting regions compared with 3R-tau (*10*). However, the results here indicate that FLNA may contribute to the pathogenesis of PSP by increasing the amount of total tau protein irrespective of each isoform.

In FLNA-Tg mice, neurons overexpressing FLNA were mainly located in deep cortical layers potentially due to impaired neural migration, where phosphorylated tau aggregated. Considering that tau is colocalized with FLNA in the NFTs in PSP, this observation in FLNA-Tg mice seems to reflect predominant tau pathology in the cortical layers IV and V (*33*). In FLNA-Tg mice, FLNA was highly expressed in the neurons and, to a lesser extent, in astrocytes and oligdendrocytes. This may explain that only a part of glial cells contains phosphorylated tau aggregates, which was less prominent than that of GFP–4R-tau in the cultured primary astrocytes or astrocytes in P7 brains of mice co-overexpressing FLNA and GFP–4R-tau.

Most sporadic PSP brains, in the absence of genetic variations in *FLNA*, showed FLNA abundance at the protein levels. While various molecules are regulated by FLNA, only a few regulators of FLNA gene expression have been identified (*23*). A previous report demonstrated that the activation of the MAPK kinase 1 (MEK1)–extracellular signal–regulated kinase 1 and 2 (ERK1/2) signaling pathway increases FLNA expression in neurons (*25*), so potentially contributes to the pathogenesis of PSP. This notion is supported by the MEK1-ERK1/2 pathway activation in the affected neurons in PSP brains (*34*, *35*). Protein kinase R–like endoplasmic reticulum kinase (PERK), encoded by *EIF2AK3*, interacts with FLNA and the subsequent F-actin in response to endoplasmic reticulum stress (*36*). A common variant at *EIF2AK3* locus is one of four risk loci for PSP identified by previous large-scale genome-wide association studies (*37*, *38*), and PERK has been found to be activated in the affected neurons of PSP brains (*39*, *40*). It still remains unclear how the protein levels of FLNA are elevated in the PSP brains, especially in the cases of no genetic variation in *FLNA*, but MEK1-ERK1/2-FLNA pathway or PERK-FLNA interaction may underlie the mechanism of up-regulation of FLNA in the PSP.

The increased tau levels in the LCLs of PSP with *FLNA* duplication and in primary cortical neurons from FLNA-Tg mice were corrected by suppression of the expression of FLNA. This suggests the potential for FLNA-targeted strategies in PSP. Amyloid-β alters protein conformation of FLNA, and the altered FLNA interacts with α7 nicotinic acetylcholine receptor and induces hyperphosphorylation of tau (*41*). A small molecule with high affinity to the altered FLNA can inhibit this amyloid-β–related pathway and tau phosphorylation (*42*). Although the application of these molecules to PSP, where is not associated with amyloid-β pathology, would be challenging, analysis of the conformation of FLNA in PSP should help drug discovery and drug repositioning. In addition, a recent proteomics study of a mouse model of AD has shown that an *N*-methyl-D-aspartate receptor antagonist memantine, a clinically approved drug for AD, reduced FLNA expression by nearly half in the hippocampus (*43*), which is expected to suppress the FLNA-driven tau aggregations.

This study underscores the potential of FLNA as a driver for tau aggregation and suggests that FLNA would be a determinant factor in PSP-tau pathology. Strategies aimed at inhibiting FLNA-driven tau aggregations could stand as a disease-modifying therapy to combat devastating neurodegeneration observed in PSP.

MATERIALS AND METHODS

Human brains

We subjected 52 autopsied individuals to the study, which comprised 11 cases with PSP, 12 with CBD, 11 with AD, 6 with PD, 5 with DLB, 2 with PiD, and 5 normal control subjects who died without any evidence of central nervous system disorders. Frontal lobe samples were used for biochemical analysis. All autopsied cases were obtained from the Brain Bank of the Institute for Medical Science of Aging, Aichi Medical University. The demography of the twins with PSP and other autopsied subjects is shown in fig. S4 and table S2. Neuropathological diagnosis of PSP (*44*), CBD (*45*), AD (*46*), PD (*47*), and DLB (*48*) was made in accordance with the published guidelines. PiD was defined as having frontal temporal dementia symptoms (*49*) and 3R-tau–immunopositive Pick bodies. Age-related pathologies were consistently assessed in the autopsied subjects: Braak NFT staging (graded from 0, I to VI) (*50*), AT8 staging (graded from 0, I to VI) (*51*), argyrophilic grain staging (graded from 0, I to III) (*52*), and Consortium to Establish a Registry for Alzheimer's Disease score (graded from 0, A to C) (*53*). We isolated genomic DNA from blood leukocytes of Twin-A, Twin-B, and their three siblings (II-1 to II-3) and frozen brain tissues of the autopsied PSP subjects (PSP-1 to PSP-9) from the Brain Bank. All individuals agreed to participate in the study, and the biological samples were obtained after written informed consent from brain donors and/or next of kin. The study adhered to the Ethical Guidelines for Human Genome/Gene Analysis Research and those for Medical and Health Research Involving Human Subjects by Japanese government and use of human biological samples was approved by the Ethics Review Committees of Nagoya University, Aichi Medical University, Niigata University, and Yokohama City University. Frontal lobe samples were snap-frozen in liquid nitrogen and stored at −80°C for later biochemical analysis.

Animal

The rTg4510 mice (stock no. 024854), which overexpress P301L mutant tau, and humanized tau mice (TAU KO; hT-PAC-N. stock

no. 36116-JAX) were obtained from the Jackson Laboratory. All wild-type or transgenic C57BL/6 mice, ICR mice, and Wistar rats used in this study were purchased from Japan SLC. All animal experiments were performed in accordance with the National Institutes of Health *Guide for the Care and Use of Laboratory Animals* and with the approval of the Nagoya University Animal Experiment Committee.

Mice for IUE

We performed IUE as described previously with modifications (*54*–*56*). Briefly, we injected 1.0 μg of each plasmid DNA solution into the right lateral ventricle of E14 ICR mouse embryos. The head of the embryo inside the uterus was placed between the disks of a forceps-type electrode (3-mm disk electrodes, CUY650P3, Nepa Gene), and electric pulses (32 V; pulse on, 50 ms; pulse off, 450 ms) were applied five times.

Primary astrocyte culture

We extracted and cultured rat primary astrocytes as previously described (*57*). Briefly, the cerebral cortex was taken from P1 of Wistar rats and incubated in Hanks' balanced salt solution with 0.25% trypsin and deoxyribonuclease I (DNase I) at 37°C for 15 min. Cortical cells from one rat were plated on a T-75 flask with Dulbecco's modified Eagle's medium (Nakarai Tesque) with 20% fetal bovine serum (FBS). The medium was replaced to the fresh medium every 3 days. When cells became confluent, the flask of mix glial cells was shaken for overnight at 200 rpm to eliminate microglial cells and oligodendrocytes. Trypsinized astrocytes were transferred into collagen-coated chamber slides and six-well dishes, infected with lentivirus for expression of GFP–4R-tau, and then used for immunocytochemistry and immunoblots. We used Lipofectamine 3000 (Invitrogen) as a plasmid transfection reagent for the primary astrocytes.

Primary cortical neuron culture

We extracted and cultured primary cortical neurons from E15 ICR mouse brains that had been electroporated at E14 or E18 FLNA-Tg mouse brains. The cerebral cortex was mechanically dissociated using neuron dissociation solutions (Fujifilm). Neurons were plated at a density of 1.5×10^5 cells in poly-D-lysine–coated chamber slides (Corning) with neuron culture medium (Fujifilm).

Sarkosyl-insoluble fractions

Sarkosyl-insoluble fractions were taken from the frozen frontal lobes and the HEK293 cells transfected with the indicated plasmids by a slightly modified method described previously (*58*). Briefly, the cells and tissues were homogenized in 10 volumes of TBS [50 mM tris/HCl (pH 8.0), 274 mM NaCl, 5 mM KCl, protease inhibitor cocktail (Roche, 1 tablet per 10 ml), and phosphatase inhibitor (Roche, 1 tablet per 10 ml)]. The homogenates were centrifuged at 27,000*g* for 20 min at 4°C to obtain TBS-extractable supernatant fractions (S1) and TBS-insoluble pellet fractions (P1). The P1 pellets were homogenized in five volumes of high-salt/sucrose buffer [0.8 M NaCl, 10% sucrose, 10 mM tris/HCl, (pH 7.4), 1 mM EDTA, protease inhibitor cocktail, and phosphatase inhibitor] and centrifuged as above. The high-salt supernatant fractions (S2) were collected and incubated with sarkosyl (1% final concentration; Sigma-Aldrich) for 1 hour at 37°C, followed by centrifugation at 150,000*g* for 1 hour at 4°C to obtain high-salt and sarkosyl-extractable fractions (S3) and sarkosyl-insoluble fractions (P3). The pellets of P3 were resuspended in Tris-EDTA Buffer [10 mM tris/HCl (pH 8.0), and 1 mM EDTA] to a volume equivalent to half of that of the brain specimens used to produce brain homogenates.

Protein identification by nanoLC-MS/MS

The proteins in P3 from PSP or normal control brains were separated by SDS-PAGE using 5 to 20% polyacrylamide gel (Fujifilm) and visualized by silver stain (Fujifilm). The PSP-specific protein bands were excised from the gels, reduced using 100 mM dithiothreitol, and alkylated with 100 mM iodoacetamide. After washing, the gels were incubated with trypsin overnight at 30°C. Recovered peptides were desalted on a ZipTip C18 (Merck). Samples were analyzed on a nanoLC-MS/MS system (Sciex). Mass data acquisition was piloted by Mascot software (https://proteomicsresource.washington.edu/mascot/) by Japan Proteomics.

Zygosity

To confirm monozygosity in Twin-A and Twin-B, we genotyped 12 microsatellite markers using fluorescent-labeled primers obtained from the ABI PRISM Linkage Mapping Set version 2.5 (Applied Biosystems).

Lymphoblast cell lines

Epstein-Barr virus–immortalized LCLs were generated from the peripheral blood B cells from Twin-A, Twin-B, and their three siblings (II-1 to II-3). These LCLs were cultured in T-75 flasks using RPMI 1640 (Gibco) medium supplemented with 10% FBS at 37°C and 5% CO_2 in a humidified incubator.

Whole-exome sequencing

We performed whole-exome sequencing (WES) for genomic DNA from Twin-A. Genomic DNA was captured using a SureSelect Human All Exon V6 kit (Agilent Technologies). Samples were sequenced on HiSeq2500 (Illumina) with 101–base pair paired-end reads. Illumina's HiSeq Control Software was used for sequencing and real-time analysis, followed by Consensus Assessment of Sequence and Variation procedure for base calling and demultiplexing. Reads were aligned to GRCh37 using Novoalign (http://novocraft.com/). PCR duplicates were removed using Picard (http://picard.sourceforge.net/). Local realignments around indels and base quality score recalibration were performed using the Genome Analysis Toolkit (GATK), and analysis-ready BAM files were generated. Using the BAM files, variants were called by the GATK UnifiedGenotyper and filtered according to GATK Best Practices (https://software.broadinstitute.org/gatk/). The common variants registered in dbSNP137 (minor allele frequency ≥ 0.01) without known clinical associations were excluded for further analysis. Included variants were annotated using ANNOVAR (http://annovar.openbioinformatics.org/). The WES mean coverage depth against RefSeq coding sequence was 69.7×, and 95.1% of total coding sequence bases were covered by 20 reads or more.

Copy number variant analysis

We used eXome Hidden Markov Model (XHMM) v1.0 for WES-based copy number variant (CNV) analysis as previously described (*59*, *60*). Briefly, we first generated analysis-ready BAM files of Twin-A plus 513 Japanese healthy males. The mean depth of each sequencing target in each sample was calculated from the BAM files using GATK DepthOfCoverage function and merged into a

samples-by-target matrix. Sequencing targets with extreme GC content, low sequence complexity, extreme size, and/or extreme mean depth were removed; samples with extreme mean and/or SD of depth were removed. The depth in the matrix was mean-centered in each target, and principal components (PCs) analysis was performed. The top PCs were removed from the matrix, and the *z* score of each target relative to all targets in each sample was calculated. From the z scores, CNVs were called using the HMM algorithm. The *z* scores were visualized with SignalMap version 1.9.0.05 (Roche Nimblegen). To confirm copy number change in suspected CNVs, we performed high-resolution chromosome microarray and qRT-PCR as follows.

High-resolution chromosome microarray

We genotyped the twins and their siblings on high-resolution chromosome microarray platforms for the detection of CNVs using the CytoScan Reagent Kit, CytoScan Amplification Kit, and CytoScanHD Array (Affymetrix). Briefly, genomic DNA was purified with ethanol precipitation. The 250 ng of the purified genomic DNA was digested with Nsp I, ligated to adaptor with T4 DNA ligase, and PCR-amplified with Titanium Taq DNA Polymerase primers targeting the adaptor sequence. The amplicon was purified with magnetic beads, fragmentated with DNase I, and biotin-labeled with terminal deoxynucleotidyl transferase. The labeled DNA was hybridized to CytoScan HD Chip in Gene Chip Hybridization Oven 640 (Affymetrix) with hybridization buffer. The chip was washed and scanned with GeneChip Fluidics Station 450 (Affymetrix). Data were analyzed using Chromosome Analysis Suitesoftware version 1.2.0.225 (Affymetrix).

Rare variant association analysis

WES was performed on 312 Japanese cases with PSP, 71 cases with CBD, 141 cases with AD, and 499 Japanese control subjects (table S4). The cases with PSP were composed of 199 participants who were clinically diagnosed in the cohort of the Japanese Longitudinal Biomarker Study in PSP and CBD (JALPAC) and 113 autopsy cases. We selected protein-altering variants located in the FLNA that met the following criteria: (i) passing variant filters, (ii) call rate $\geq$ 95%, (iii) quality by depth $\geq$ 3, (iv) inbreeding coefficient $\geq$ −0.3, (v) combined annotation dependent depletion (CADD) score $\geq$ 10, and (vi) proportion expressed across transcripts (pext) score (*61*) of substantia nigra $\geq$ 0.1 if available. To obtain rare variants, we further narrowed down to variants with a maximum allele frequency of less than 1% in each ethnic population with more than 1000 subjects using publicly available databases: ExAC release 0.3, gnomAD release 2.1.1 for exomes and r.3.0 for genomes (the following URL for both of ExAC and gnomAD; https://gnomad.broadinstitute.org/), HGVD version 2.3 (www.hgvd.genome.med.kyoto-u.ac.jp/), and ToMMo version 8.3KJPN (https://jmorp.megabank.tohoku.ac.jp).

Reverse transcription of total RNA

We isolated total RNA from cells using the miRNeasy Mini Kit (QIAGEN) and then reverse-transcribed 1.0 μg of RNA from each sample into cDNA using oligo(dT) priming and the ImProm-II Reverse Transcription System (Promega).

Quantitative real-time polymerase chain reaction

All qRT-PCR reactions were performed in a 96-well plate format on a CFX96 system (Bio-Rad) using THUNDERBIRD SYBR qPCR Mix (Toyobo). See table S6 for a list of primer sets. For the thermal cycle reaction, a CFX96 system (Bio-Rad) was used at 95°C for 3 min and then 40 cycles at 95°C for 10 s and 55°C for 30 s. Relative quantification of gene expression was calculated by the $2-\Delta\Delta C_t$ method using housekeeping genes as reference and control samples (as specified in the figure legends) as calibrator. qRT-PCR was performed in triplicate for each sample, after which all experiments were repeated twice.

XCI analysis

We performed XCI analysis using *FRAXA* locus methylation assay as previously described (*62*). Briefly, genomic DNA from the subjects was digested with two methylation-sensitive enzymes, Hpa II and Hha I (Takara). The digested DNA was PCR-amplified with fluorescent-labeled primers targeting a triplet repeat of *FRAXA* gene. See table S6 for a list of primer sets. Fluorescent-labeled products were analyzed on an ABI PRISM 3500 Genetic Analyzer with GeneMapper Software version 4.0 (Applied Biosystems). X-inactivation ratios of less than or equal to 80:20 were considered to represent a random pattern, ratios greater than 80:20 were considered to represent a skewed pattern, and ratios greater than 90:10 were considered to represent a markedly skewed pattern. Fragment length along with an appropriate standard was determined using a 3730xl DNA Analyzer (Applied Biosystems) and analyzed with Peak Scanner Software 2 (Applied Biosystems).

Construction of DNA plasmids

We generated expression vectors encoding wild-type FLNA (mCherry-FLNA^{WT}), p.Ala39Gly mutant FLNA (mCherry-FLNA^{Ala39Gly}), N-terminal trancated FLNA (mCherry-FLNA$^{ABD + Ig1–15}$), C-terminal trancated FLNA (mCherry-FLNA$^{Ig16–24}$), Ig1-8 domain of FLNA (mCherry-FLNA$^{Ig1–8}$), Ig9-15 domain of FLNA (mCherry-FLNA$^{Ig9–15}$), Ig16-23 domain of FLNA (mCherry-FLNA$^{Ig16-23}$), truncated version of FLNA deleting Ig16-23 (mCherry-FLNA$^{ABD + Ig1-15+ Ig24}$), truncated version of FLNA deleting Ig1-8 and Ig16-23 (mCherry-FLNA$^{ABD + Ig9-15+ Ig24}$: ΔFLNA), p.Ser2523Asn rare variant FLNA (mCherry-FLNA^{Ser2523Asn}), p.Arg2334Cys rare variant FLNA (mCherry-FLNA^{Arg2334Cys}), p.Val2191Met rare variant FLNA (mCherry-FLNA^{Val2191Met}), p.Ala2075Ser rare variant FLNA (mCherry-FLNA^{Ala2075Ser}), p.Arg2003His rare variant FLNA (mCherry-FLNA^{Arg2003His}), p.Leu1980Val rare variant FLNA (mCherry-FLNA^{Leu1980Val}), p.Ser2523Ala non-phosphorylated variant FLNA (mCherry-FLNA^{Ser2523Ala}), and mCherry (mCherry-empty) from mCherry-FilaminA-N-9 (Addgene, plasmid 55047) for in vitro assays. Next, we subcloned the wild-type or mutant *FLNA* sequence, inserted the pCAG-Neo (Wako), and generated pCAG-FLNA^{WT} or pCAG-FLNA^{Ala39Gly} for in vivo assays. We inserted annealed oligonucleotides for three nuclear localization sequence (3NLS) into pCAG-mCherry (mCherry-3NLS) to label the nucleus in electroporated cells by IUE. We also generated pAAV-ΔFLNA-6xHis and pAAV-empty-6xHis from pAAV-FLEX-GFP (Addgene, plasmid 28304).

For tau overexpression, we used either pDEST12.2 vector or pLenti CMV Neo vector encoding GFP-tagged human 0N4R tau (GFP–4R-tau) and 0N3R tau (GFP–3R-tau), as described previously (*5*). *RPL10*, *GDI1*, *FAM3A*, and *G6PD* cDNA fragments were respectively amplified from these expression vectors (OHu6031, OHu19497, OHu14263, and OHu27509, GenScript) and inserted into the mCherry-empty.

Cell line culture and plasmid transfection

We cultured HEK293 cell line [American Type Culture Collection (ATCC)] in Dulbecco's modified Eagle's medium supplemented

with 10% FBS in 5% CO_2 at 37°C. We used Lipofectamine 2000 (Invitrogen) as a plasmid transfection reagent for HEK293 cells. The cells were cultured for 48 hours and then harvested before being processed for immunoblots.

Small interfering RNA

All siRNAs were purchased from Invitrogen. ID numbers are as follows: *FLNA* siRNA #1 (s5275), *FLNA* siRNA #2 (s5276), *FLNA* siRNA #3 (s5277), ribosomal protein L10 (*RPL10*) siRNA (s194740), and a negative-control siRNA (Silencer Negative Control siRNA No.1, 4390843). We transfected these siRNAs into LCLs using an electroporation system (Neon, Invitrogen). Electroporation was done according to the manufacturer using 1 pulse 30 ms at 1350 V. The transfected LCLs were cultured in T-25 flasks for 24 hours before being processed for immunoblots.

CHX chase assay

We performed CHX chase assay for tau protein stability in cell cultures as previously described (*63*). Briefly, we cotransfected the GFP–4R-tau and FLNA constructs into HEK293 cells and added CHX (100 μg/ml; Wako) to stop new protein synthesis. The cells were harvested at each time point, and the lysates were analyzed by immunoblots. The levels of GFP–4R-tau are normalized to those of glyceraldehyde-3-phosphate dehydrogenase (GAPDH) at 0 hour.

Co-immunoprecipitation

We plated HEK293 cells onto 100-mm dishes and cotransfected each dish with 8.0 μg of the vectors coexpressing GFP–4R-tau and FLNA. Forty-eight hours after the transfection, cells were harvested using trypsin-EDTA (Gibco), washed four times in phosphate-buffered saline, and lysed using Cell Lysis Buffer M (Wako). We performed immunoprecipitation using an antibody against total tau (TAU-5) (5.0 μg per sample), a mouse normal control IgG (5.0 μg per sample), and the Dynabeads Protein G Immunoprecipitation Kit (Invitrogen) according to the manufacturer's suggested protocols.

Lentivirus

Lentivirus expressing GFP–4R-tau was prepared as previously described (*5*). Briefly, lentiviral particles were produced in mycoplasma-free HEK293T cell line (ATCC) by transfection with the lentiviral plasmids and lentiviral packaging plasmids using Lipofectamine 2000 (Invitrogen). A lentivirus-containing supernatant was collected 48 hours after transfection and stored at −80°C. Lentivirus expressing short hairpin RNAs (shRNAs) were purchased from The RNAi Consortium. ID numbers are as follows: pLKO.1-puro-human *FLNA* shRNA #1 (TRCN0000062529), *FLNA* shRNA #2 (TRCN0000062532), and a negative-control siRNA (pLKO.1-puro nonmammalian shRNA control, SHC016V).

F/G actin assay

F/G-actin ratio was determined using the G-actin/F-actin In Vivo Assay Biochem Kit according to the manufacturer's instructions (Cytoskeleton Inc). Briefly, HEK293 cells expressing the indicated proteins were collected and lysed in ready-made lysis buffer. After removal of debris by centrifugation at 350*g* for 5 min, lysates were subjected to ultracentrifugation at 100,000*g* for 1 hour to separate the pellet from soluble supernatant (G-actin). An equal amount of ready-made F-actin depolymerization buffer containing urea was added to the pellet containing F-actin. An equal amount of both suspensions was used for immunoblots using anti-actin antibody.

Live imaging for F-actin dynamics in cortical slice culture

For live imaging of F-actin in neurons in the mouse cerebral wall, pCAG-LPL-Lifeact-EGFP (enhanced GFP) (0.5 μg/μl) and pEFX-Cre (0.002 μg/μl) were transfected together with pCAG-FLNA (1.0 μg/μl) or pCAG-empty vector (1.0 μg/μl) by IUE. To visualize F-actin dynamics in neurons, electroporation was performed at E14 and then at E17, which is the timing that electroporated cells differentiate into neurons, and cerebral walls were microsurgically processed to make slices. Cortical slices were embedded in type I collagen gel solution (the final concentration: 0.7 to 0.8 mg/ml; Cellmatrix I-A, Nitta Gelatin) on a polystyrene cell culture dish (Corning). Time-lapse imaging data were collected using CSU-X1 laser scanning confocal microscopy (Yokogawa Electric Corporation) with a 100× objective lens (LUMPLFL100XW, Olympus). Chambers for on-stage culture were filled with 45% N_2, 40% O_2, and 5% CO_2.

Stereotaxic injection of AAV vector

AAV vectors were prepared by CsCl density gradient ultracentrifugation as previously described (*64*). Mice were deeply anesthetized and immobilized in a stereotaxic frame. All mice were injected using a Hamilton syringe with either AAV-ΔFLNA or AAV-empty at a concentration of 1.0×10^9 viral genomes/μl into frontal lobes (anterior-posterior, +1.61 mm; medial-lateral, ±2.58 mm; and dorsal-ventral, −1.55 mm).

Generation of human FLNA transgenic mice

The CAG promoter–driven and FLAG-tagged human FLNA fragments with bovine growth hormone (bGH) polyadenylate [poly(A)] signals were prepared by digestion of PshB I sites in pCAG-FLNA^{WT} vectors. We generated transgenic mice by microinjection into C57BL/6 fertilized eggs and obtained the founders with human FLNA.

Immunoblot

We performed immunoblots as previously described (*65*). See table S6 for a list of antibodies. GAPDH serves as a loading control. An LAS3000 imaging system (Fujifilm) was used to produce digital images. The signal intensities of these independent blots were quantified using Image Gauge Software version 4.22 (Fujifilm) and expressed in arbitrary units.

Immunohistochemistry

We performed immunohistochemistry as previously described (*55*, *65*). Briefly, the frozen sections were incubated for 20 min at 70°C in HistoVT One (Nacalai) for antigen retrieval. The paraffin sections were deparaffinized, rehydrated, and then heated in a microwave for 15 min in 10 mM citrate buffer at pH 6. The sections were incubated with Tris-NaCl-blocking buffer (PerkinElmer) for 20 min at room temperature, primary antibodies overnight at 4°C, and fluorescent secondary antibodies for 30 min at room temperature. Between all steps, the sections were washed with phosphate-buffered saline without detergent three times. See table S6 for a list of antibodies. An EnVision+ System containing horseradish peroxidase (Dako) was used for 3,3′-diaminobenzidine staining. Image data were collected using LSM710 laser scanning confocal microscope (Carl Zeiss) or BZ-X710 fluorescent microscope (Keyence).

Statistics

All biological experiments were performed repeatedly at least twice. Sample size were determined on the basis of whether data are

reproducible in independent sets of experiments. Typically, three independent experiments were used to determine the reproducibility of data. Samples were randomly chosen. Blinding was not possible in this study, so we prepared both control and tested samples at the same time for each independent set of experiments. No data were arbitrarily excluded from the experiments. Statistical analysis was performed using R version 3.5.1 (https://r-project.org), a software for bioinformatics. Student's *t* tests or Welch's *t* tests were performed for pairwise comparison, while multiple data groups were analyzed by analysis of variance (ANOVA) with Tukey-Kramer post hoc test. Association study was analyzed with Fisher's exact test. All values are presented as means ± SEM. A P value less than 0.05 was considered significant: $^{***}P < 0.001$, $^{**}P < 0.01$, and $^{*}P < 0.05$.

SUPPLEMENTARY MATERIALS

Supplementary material for this article is available at https://science.org/doi/10.1126/sciadv.abm5029

View/request a protocol for this paper from *Bio-protocol*.

REFERENCES AND NOTES

1. A. L. Boxer, J. T. Yu, L. I. Golbe, I. Litvan, A. E. Lang, G. U. Höglinger, Advances in progressive supranuclear palsy: New diagnostic criteria, biomarkers, and therapeutic approaches. *Lancet Neurol.* **16**, 552–563 (2017).
2. B. Uttl, P. Santacruz, I. Litvan, J. Grafman, Caregiving in progressive supranuclear palsy. *Neurology* **51**, 1303–1309 (1998).
3. S. A. Glasmacher, P. N. Leigh, R. A. Saha, Predictors of survival in progressive supranuclear palsy and multiple system atrophy: A systematic review and meta-analysis. *J. Neurol. Neurosurg. Psychiatry* **88**, 402–411 (2017).
4. M. Yoshida, Astrocytic inclusions in progressive supranuclear palsy and corticobasal degeneration. *Neuropathology* **34**, 555–570 (2014).
5. S. Ishigaki, Y. Fujioka, Y. Okada, Y. Riku, T. Udagawa, D. Honda, S. Yokoi, K. Endo, K. Ikenaka, S. Takagi, Y. Iguchi, N. Sahara, A. Takashima, H. Okano, M. Yoshida, H. Warita, M. Aoki, H. Watanabe, H. Okado, M. Katsuno, G. Sobue, Altered tau isoform ratio caused by loss of FUS and SFPQ function leads to FTLD-like phenotypes. *Cell Rep.* **18**, 1118–1131 (2017).
6. S. Ishigaki, Y. Riku, Y. Fujioka, K. Endo, N. Iwade, K. Kawai, M. Ishibashi, S. Yokoi, M. Katsuno, H. Watanabe, K. Mori, A. Akagi, O. Yokota, S. Terada, I. Kawakami, N. Suzuki, H. Warita, M. Aoki, M. Yoshida, G. Sobue, Aberrant interaction between FUS and SFPQ in neurons in a wide range of FTLD spectrum diseases. *Brain* **143**, 2398–2405 (2020).
7. M. B. Delisle, J. R. Murrell, R. Richardson, J. A. Trofatter, O. Rascol, X. Soulages, M. Mohr, P. Calvas, B. Ghetti, A mutation at codon 279 (N279K) in exon 10 of the tau gene causes a tauopathy with dementia and supranuclear palsy. *Acta Neuropathol.* **98**, 62–77 (1999).
8. F. Liu, C. X. Gong, Tau exon 10 alternative splicing and tauopathies. *Mol. Neurodegen.* **3**, 8 (2008).
9. J. Vandewalle, H. van Esch, K. Govaerts, J. Verbeeck, C. Zweier, I. Madrigal, M. Mila, E. Pijkels, I. Fernandez, J. Kohlhase, C. Spaich, A. Rauch, J. P. Fryns, P. Marynen, G. Froyen, Dosage-dependent severity of the phenotype in patients with mental retardation due to a recurrent copy-number gain at Xq28 mediated by an unusual recombination. *Am. J. Hum. Genet.* **85**, 809–822 (2009).
10. Y. Cabrales Fontela, H. Kadavath, J. Biernat, D. Riedel, E. Mandelkow, M. Zweckstetter, Multivalent cross-linking of actin filaments and microtubules through the microtubule-associated protein tau. *Nat. Commun.* **8**, 1981 (2017).
11. F. Nakamura, T. M. Osborn, C. A. Hartemink, J. H. Hartwig, T. P. Stossel, Structural basis of filamin A functions. *J. Cell Biol.* **179**, 1011–1025 (2007).
12. D. V. Iwamoto, A. Huehn, B. Simon, C. Huet-Calderwood, M. Baldassarre, C. V. Sindelar, D. A. Calderwood, Structural basis of the filamin A actin-binding domain interaction with F-actin. *Nat. Struct. Mol. Biol.* **25**, 918–927 (2018).
13. Y. Ohta, J. H. Hartwigm, Actin filament cross-linking by chicken gizzard filamin is regulated by phosphorylation in vitro. *Biochemistry* **34**, 6745–6754 (1995).
14. T. Borbiev, A. D. Verin, S. Shi, F. Liu, J. G. N. Garcia, Regulation of endothelial cell barrier function by calcium/calmodulin-dependent protein kinase II. *Am. J. Physiol. Lung Cell. Mol. Physiol.* **280**, 983–990 (2001).
15. V. Graham, J. Khudyakov, P. Ellis, L. Pevny, SOX2 functions to maintain neural progenitor identity. *Neuron* **39**, 749–765 (2003).
16. E. A. Alcamo, L. Chirivella, M. Dautzenberg, G. Dobreva, I. Fariñas, R. Grosschedl, S. K. McConnell, Satb2 regulates callosal projection neuron identity in the developing cerebral cortex. *Neuron* **57**, 364–377 (2008).
17. P. McMillan, E. Korvatska, P. Poorkaj, Z. Evstafjeva, L. Robinson, L. Greenup, J. Leverenz, G. D. Schellenberg, I. D'Souza, Tau isoform regulation is region- and cell-specific in mouse brain. *J. Comp. Neurol.* **511**, 788–803 (2008).
18. W. Zhang, S. W. Han, D. W. Mckeel, A. Goate, J. Y. Wu, Interaction of presenilins with the filamin family of actin-binding proteins. *J. Neurosci.* **18**, 914–922 (1998).
19. S. Feuillette, V. Deramecourt, A. Laquerriere, C. Duyckaerts, M. B. Delisle, C. A. Maurage, D. Blum, L. Buée, T. Frébourg, D. Campion, M. Lecourtois, Filamin-A and myosin VI colocalize with fibrillary Tau protein in Alzheimer's disease and FTDP-17 brains. *Brain Res.* **1345**, 182–189 (2010).
20. S. Oddo, A. Caccamo, J. D. Shepherd, M. P. Murphy, T. E. Golde, R. Kayed, R. Metherate, M. P. Mattson, Y. Akbari, F. M. Laferla, Triple-transgenic model of Alzheimer's disease with plaques and tangles: Intracellular A and synaptic dysfunction. *Neuron* **39**, 409–421 (2003).
21. C. Ballatore, V. M. Y. Lee, J. Q. Trojanowski, Tau-mediated neurodegeneration in Alzheimer's disease and related disorders. *Nat. Rev. Neurosci.* **8**, 663–672 (2007).
22. A. X. Zhou, J. H. Hartwig, L. M. Akyürek, Filamins in cell signaling, transcription and organ development. *Trends Cell Biol.* **20**, 113–123 (2010).
23. R. M. Savoy, P. M. Ghosh, The dual role of filamin A in cancer: Can't live with (too much of) it, can't live without it. *Endocr. Relat. Cancer* **20**, R341–R356 (2013).
24. J. W. Fox, E. D. Lamperti, Y. Z. Ekşioğlu, S. E. Hong, Y. Feng, D. A. Graham, I. E. Scheffer, W. B. Dobyns, B. A. Hirsch, R. A. Radtke, S. F. Berkovic, P. R. Huttenlocher, C. A. Walsh, Mutations in filamin 1 prevent migration of cerebral cortical neurons in human periventricular heterotopia. *Neuron* **21**, 1315–1325 (1998).
25. L. Zhang, C. M. Bartley, X. Gong, L. S. Hsieh, T. V. Lin, D. M. Feliciano, A. Bordey, MEK-ERK1/2-dependent FLNA overexpression promotes abnormal dendritic patterning in tuberous sclerosis independent of mTOR. *Neuron* **84**, 78–91 (2014).
26. T. A. Fulga, I. Elson-Schwab, V. Khurana, M. L. Steinhilb, T. L. Spires, B. T. Hyman, M. B. Feany, Abnormal bundling and accumulation of F-actin mediates tau-induced neuronal degeneration in vivo. *Nat. Cell Biol.* **9**, 139–148 (2007).
27. F. H. Bardai, L. Wang, Y. Mutreja, M. Yenjerla, T. C. Gamblin, M. B. Feany, A conserved cytoskeletal signaling cascade mediates neurotoxicity of FTDP-17 tau mutations in vivo. *J. Neurosci.* **38**, 108–119 (2018).
28. C. Spanaki, H. Latsoudis, A. Plaitakis, LRRK2 mutations on Crete: R1441H associated with PD evolving to PSP. *Neurology* **67**, 1518–1519 (2006).
29. M. Sanchez-Contreras, M. G. Heckman, P. Tacik, N. Diehl, P. H. Brown, A. I. Soto-Ortolaza, E. A. Christopher, R. L. Walton, O. A. Ross, L. I. Golbe, N. Graff-Radford, Z. K. Wszolek, D. W. Dickson, R. Rademakers, Study of LRRK2 variation in tauopathy: Progressive supranuclear palsy and corticobasal degeneration. *Mov. Disord.* **32**, 115–123 (2017).
30. C. Blauwendraat, O. Pletnikva, J. T. Geiger, N. A. Murphy, Y. Abramzon, G. Rudow, A. Mamais, M. S. Sabir, C. B. Crain, S. Ahmed, L. S. Rosenthal, C. C. Bakker, F. Faghri, R. Chia, J. Ding, T. M. Dawson, A. Pantelyat, M. S. Albert, M. A. Nalls, S. M. Resnick, L. Ferrucci, M. R. Cookson, A. E. Hillis, J. C. Troncoso, S. W. Scholz, Genetic analysis of neurodegenerative diseases in a pathology cohort. *Neurobiol. Aging* **76**, 214.e1–214.e9 (2019).
31. F. H. Bardai, D. G. Ordonez, R. M. Bailey, M. Hamm, J. Lewis, M. B. Feany, Lrrk promotes tau neurotoxicity through dysregulation of actin and mitochondrial dynamics. *PLOS Biol.* **16**, e2006265 (2018).
32. Y. Tsuboi, J. Slowinski, K. A. Josephs, W. G. Honer, Z. K. Wszolek, D. W. Dickson, Atrophy of superior cerebellar peduncle in progressive supranuclear palsy. *Neurology* **60**, 1766–1769 (2003).
33. M. Verny, C. Duyckaerts, Y. Agid, J. J. Hauw, The significance of cortical pathology in progressive supranuclear palsy clinico-pathological data in 10 cases. *Brain* **119**, 1123–1136 (1996).
34. I. Ferrer, R. Blanco, M. Carmona, B. Puig, Phosphorylated mitogen-activated protein kinase (MAPK/ERK-P), protein kinase of 38kDa (p38-P), stress-activated protein kinase (SAPK/JNK-P), and calcium/calmodulin-dependent kinase II (CaM kinase II) are differentially expressed in tau deposits in neurons and glial cells in tauopathies. *J. Neural Transm. (Vienna)* **108**, 1397–1415 (2001).
35. I. Ferrer, R. Blanco, M. Carmona, R. Ribera, E. Goutan, B. Puig, M. J. Rey, A. Cardozo, F. Viñals, T. Ribalta, Phosphorylated map kinase (ERK1, ERK2) expression is associated with early tau deposition in neurones and glial cells, but not with increased nuclear DNA vulnerability and cell death, in Alzheimer disease, Pick's disease, progressive supranuclear palsy and corticobasal degeneration. *Brain Pathol.* **11**, 144–158 (2001).
36. A. R. van Vliet, F. Giordano, S. Gerlo, I. Segura, S. van Eygen, G. Molenberghs, S. Rocha, A. Houcine, R. Derua, T. Verfaillie, J. Vangindertael, H. de Keersmaecker, E. Waelkens, J. Tavernier, J. Hofkens, W. Annaert, P. Carmeliet, A. Samali, H. Mizuno, P. Agostinis, The ER stress sensor PERK coordinates ER-Plasma membrane contact site formation through interaction with filamin-A and F-actin REMODELING. *Mol. Cell* **65**, 885–899.e6 (2017).
37. G. U. Höglinger, N. M. Melhem, D. W. Dickson, P. M. A. Sleiman, L.-S. Wang, L. Klei, R. Rademakers, R. de Silva, I. Litvan, D. E. Riley, J. C. van Swieten, P. Heutink, Z. K. Wszolek, R. J. Uitti, J. Vandrovcova, H. I. Hurtig, R. G. Gross, W. Maetzler, S. Goldwurm, E. Tolosa,

B. Borroni, P. Pastor; PSP Genetics Study Group, L. B. Cantwell, M. R. Han, A. Dillman, M. P. van der Brug, J. R. Gibbs, M. R. Cookson, D. G. Hernandez, A. B. Singleton, M. J. Farrer, C.-E. Yu, L. I. Golbe, T. Revesz, J. Hardy, A. J. Lees, B. Devlin, H. Hakonarson, U. Müller, G. D. Schellenberg, Identification of common variants influencing risk of the tauopathy progressive supranuclear palsy. *Nat. Genet.* **43**, 699–705 (2011).
38. R. Ferrari, M. Ryten, R. Simone, D. Trabzuni, N. Nicolaou, G. Hondhamuni, A. Ramasamy, J. Vandrovcova, M. E. Weale, A. J. Lees, P. Momeni, J. Hardy, R. de Silva, Assessment of common variability and expression quantitative trait loci for genome-wide associations for progressive supranuclear palsy. *Neurobiol. Aging* **35**, 1514.e1–1514.e12 (2014).
39. D. A. T. Nijholt, E. S. van Haastert, A. J. M. Rozemuller, W. Scheper, J. J. M. Hoozemans, The unfolded protein response is associated with early tau pathology in the hippocampus of tauopathies. *J. Pathol.* **226**, 693–702 (2012).
40. L. D. Stutzbach, S. X. Xie, A. C. Naj, R. Albin, S. Gilman, V. M. Y. Lee, J. Q. Trojanowski, B. Devlin, G. D. Schellenberg, The unfolded protein response is activated in disease-affected brain regions in progressive supranuclear palsy and Alzheimer's disease. *Acta Neuropathol. Commun.* **1**, 31 (2013).
41. L. H. Burns, H.-Y. Wang, Altered filamin A enables amyloid beta-induced tau hyperphosphorylation and neuroinflammation in Alzheimer's disease. *Neuroimmunol. Neuroinflam.* **4**, 263–271 (2017).
42. H. Y. Wang, K. Bakshi, M. Frankfurt, A. Stucky, M. Goberdhan, S. M. Shah, L. H. Burns, Reducing amyloid-related Alzheimer's disease pathogenesis by a small molecule targeting filamin A. *J. Neurosci.* **32**, 9773–9784 (2012).
43. X. Zhou, L. Wang, W. Xiao, Z. Su, C. Zheng, Z. Zhang, Y. Wang, B. Xu, X. Yang, M. P. M. Hoi, Memantine improves cognitive function and alters hippocampal and cortical proteome in triple transgenic mouse model of Alzheimer's disease. *Exp. Neurobiol.* **28**, 390–403 (2019).
44. I. Litvan, J. J. Hauw, J. J. Bartko, P. L. Lantos, S. E. Daniel, D. S. Horoupian, A. McKee, D. Dickson, C. Bancher, M. Tabaton, K. Jellinger, D. W. Anderson, Validity and reliability of the preliminary NINDS neuropathologic criteria for progressive supranuclear palsy and related disorders. *J. Neuropathol. Exp. Neurol.* **55**, 97–105 (1996).
45. D. W. Dickson, C. Bergeron, S. S. Chin, D. Horoupian, K. Ikeda, K. Jellinger, P. L. Lantos, C. F. Lippa, S. S. Mirra, M. Tabaton, J. P. Vonsattel, K. Wakabayashi, I. Litvan, Office of rare diseases neuropathologic criteria for corticobasal degeneration. *J. Neuropathol. Exp. Neurol.* **61**, 935–946 (2002).
46. T. J. Montine, C. H. Phelps, T. G. Beach, E. H. Bigio, N. J. Cairns, D. W. Dickson, C. Duyckaerts, M. P. Frosch, E. Masliah, S. S. Mirra, P. T. Nelson, J. A. Schneider, D. R. Thal, J. Q. Trojanowski, H. van Vinters, B. T. Hyman, National institute on aging-Alzheimer's association guidelines for the neuropathologic assessment of Alzheimer's disease: A practical approach. *Acta Neuropathol.* **123**, 1–11 (2012).
47. D. J. Gelb, E. Oliver, S. Gilman, Diagnostic criteria for Parkinson disease. *Arch. Neurol.* **56**, 33–39 (1999).
48. I. G. Mckeith, D. Dickson, J. Lowe, M. Emre, J. O'brien, H. Feldman, J. Cummings, J. Duda, C. Lippa, E. Perry, D. Aarsland, H. Arai, C. Ballard, B. Boeve, D. Burn, D. Costa, T. del Ser, B. Dubois, D. Galasko, S. Gauthier, C. Goetz, E. Gomez-Tortosa, G. Halliday, L. Hansen, J. Hardy, T. Iwatsubo, R. Kalaria, D. Kaufer, R. Kenny, A. Korczyn, K. Kosaka, M.-Y. Lee, A. Lees, I. Litvan, E. Londos, O. Lopez, S. Minoshima, Y. Mizuno, J. A. Molina, E. Mukaetova-Ladinska, F. Pasquier, R. H. Perry, J. B. Schulz, J. Trojanowski, M. Yamada, Diagnosis and management of dementia with Lewy bodies: Third report of the DLB Consortium. *Neurology* **65**, 1863–1872 (2005).
49. D. Neary, J. S. Snowden, L. Gustafson, U. Passant, D. Stuss, S. Black, M. Freedman, A. Kertesz, P. H. Robert, M. Albert, K. Boone, B. L. Miller, J. Cummings, D. F. Benson, Frontotemporal lobar degeneration A consensus on clinical diagnostic criteria. *Neurology* **51**, 1546–1554 (1998).
50. H. Braak, E. Braak, Neuropathological stageing of Alzheimer-related changes. *Acta Neuropathol.* **82**, 239–259 (1991).
51. H. Braak, I. Alafuzoff, T. Arzberger, H. Kretzschmar, K. Tredici, Staging of Alzheimer disease-associated neurofibrillary pathology using paraffin sections and immunocytochemistry. *Acta Neuropathol.* **112**, 389–404 (2006).
52. Y. Saito, N. N. Ruberu, M. Sawabe, T. Arai, N. Tanaka, Y. Kakuta, H. Yamanouchi, S. Murayama, Staging of Argyrophilic Grains: An age-associated tauopathy. *J. Neuropathol. Exp. Neurol.* **63**, 911–918 (2004).
53. S. Mirra, A. Heyman, D. McKeel, S. Sumi, B. Crain, L. Brownlee, F. Vogel, J. Hughes, G. van Belle, L. Berg, The Consortium to Establish a Registry for Alzheimer's Disease (CERAD). Part 11. Standardization of the neuropathologic assessment of Alzheimer's disease. *Neurology* **41**, 479–486 (1991).
54. M. Okamoto, T. Namba, T. Shinoda, T. Kondo, T. Watanabe, Y. Inoue, K. Takeuchi, Y. Enomoto, K. Ota, K. Oda, Y. Wada, K. Sagou, K. Saito, A. Sakakibara, A. Kawaguchi, K. Nakajima, T. Adachi, T. Fujimori, M. Ueda, S. Hayashi, K. Kaibuchi, T. Miyata, TAG-1-assisted progenitor elongation streamlines nuclear migration to optimize subapical crowding. *Nat. Neurosci.* **16**, 1556–1566 (2013).
55. Y. Hattori, T. Miyata, Embryonic neocortical microglia express toll-like receptor 9 and respond to plasmid DNA injected into the ventricle: Technical considerations regarding microglial distribution in electroporated brain walls. *eNeuro.* **5**, ENEURO.0312-18 (2018).
56. Y. Hattori, Y. Naito, Y. Tsugawa, S. Nonaka, H. Wake, T. Nagasawa, A. Kawaguchi, T. Miyata, Transient microglial absence assists postmigratory cortical neurons in proper differentiation. *Nat. Commun.* **11**, 1631 (2020).
57. Y. Chen, V. Balasubramaniyan, J. Peng, E. C. Hurlock, M. Tallquist, J. Li, Q. R. Lu, Isolation and culture of rat and mouse oligodendrocyte precursor cells. *Nat. Protoc.* **2**, 1044–1051 (2007).
58. N. Sahara, M. de Ture, Y. Ren, A. S. Ebrahim, D. Kang, J. Knight, C. Volbracht, J. T. Pedersen, D. W. Dickson, S. H. Yen, J. Lewis, Characteristics of TBS-extractable hyperphosphorylated tau species: Aggregation intermediates in rTg4510 mouse brain. *J. Alzheimers Dis.* **33**, 249–263 (2013).
59. M. Fromer, J. L. Moran, K. Chambert, E. Banks, S. E. Bergen, D. M. Ruderfer, R. E. Handsaker, S. A. McCarroll, M. C. O'Donovan, M. J. Owen, G. Kirov, P. F. Sullivan, C. M. Hultman, P. Sklar, S. M. Purcell, Discovery and statistical genotyping of copy-number variation from whole-exome sequencing depth. *Am. J. Hum. Genet.* **91**, 597–607 (2012).
60. M. Fromer, S. M. Purcell, Using XHMM software to detect copy number variation in whole-exome sequencing data. *Curr. Protoc. Hum. Genet.* **81**, 7.23.1–7.23.21 (2014).
61. B. B. Cummings, K. J. Karczewski, J. A. Kosmicki, E. G. Seaby, N. A. Watts, M. Singer-Berk, J. M. Mudge, J. Karjalainen, F. K. Satterstrom, A. H. O'Donnell-Luria, T. Poterba, C. Seed, M. Solomonson, J. Alföldi, J. Alföldi, I. M. Armean, E. Banks, L. Bergelson, K. Cibulskis, R. L. Collins, K. M. Connolly, M. Covarrubias, B. B. Cummings, M. J. Daly, S. Donnelly, Y. Farjoun, S. Ferriera, L. Francioli, S. Gabriel, L. D. Gauthier, J. Gentry, N. Gupta, T. Jeandet, D. Kaplan, K. J. Karczewski, K. M. Laricchia, C. Llanwarne, E. van Minikel, R. Munshi, B. M. Neale, S. Novod, A. H. O'Donnell-Luria, N. Petrillo, T. Poterba, D. Roazen, V. Ruano-Rubio, A. Saltzman, K. E. Samocha, M. Schleicher, C. Seed, M. Solomonson, J. Soto, G. Tiao, K. Tibbetts, C. Tolonen, C. Vittal, G. Wade, A. Wang, Q. Wang, J. S. Ware, N. A. Watts, B. Weisburd, N. Whiffin, C. A. A. Salinas, T. Ahmad, C. M. Albert, D. Ardissino, G. Atzmon, J. Barnard, L. Beaugerie, E. J. Benjamin, M. Boehnke, L. L. Bonnycastle, E. P. Bottinger, D. W. Bowden, M. J. Bown, J. C. Chambers, J. C. Chan, D. Chasman, J. Cho, M. K. Chung, B. Cohen, A. Correa, D. Dabelea, M. J. Daly, D. Darbar, R. Duggirala, J. Dupuis, P. T. Ellinor, R. Elosua, J. Erdmann, T. Esko, M. Färkkilä, J. Florez, A. Franke, G. Getz, B. Glaser, S. J. Glatt, D. Goldstein, C. Gonzalez, L. Groop, C. Haiman, C. Hanis, M. Harms, M. Hiltunen, M. M. Holi, C. M. Hultman, M. Kallela, J. Kaprio, S. Kathiresan, B. J. Kim, Y. J. Kim, G. Kirov, J. Kooner, S. Koskinen, H. M. Krumholz, S. Kugathasan, S. H. Kwak, M. Laakso, T. Lehtimäki, R. J. F. Loos, S. A. Lubitz, R. C. W. Ma, D. G. MacArthur, J. Marrugat, K. M. Mattila, S. McCarroll, M. I. McCarthy, D. McGovern, R. McPherson, J. B. Meigs, O. Melander, A. Metspalu, B. M. Neale, P. M. Nilsson, M. C. O'Donovan, D. Ongur, L. Orozco, M. J. Owen, C. N. A. Palmer, A. Palotie, K. S. Park, C. Pato, A. E. Pulver, N. Rahman, A. M. Remes, J. D. Rioux, S. Ripatti, D. M. Roden, D. Saleheen, V. Salomaa, N. J. Samani, J. Scharf, H. Schunkert, M. B. Shoemaker, P. Sklar, H. Soininen, H. Sokol, T. Spector, P. F. Sullivan, J. Suvisaari, E. S. Tai, Y. Y. Teo, T. Tiinamaija, M. Tsuang, D. Turner, T. Tusie-Luna, E. Vartiainen, J. S. Ware, H. Watkins, R. K. Weersma, M. Wessman, J. G. Wilson, R. J. Xavier, M. J. Daly, D. G. MacArthur, Transcript expression-aware annotation improves rare variant interpretation. *Nature* **581**, 452–458 (2020).
62. H. Saitsu, T. Nishimura, K. Muramatsu, H. Kodera, S. Kumada, K. Sugai, E. Kasai-Yoshida, N. Sawaura, H. Nishida, A. Hoshino, F. Ryujin, S. Yoshioka, K. Nishiyama, Y. Kondo, Y. Tsurusaki, M. Nakashima, N. Miyake, H. Arakawa, M. Kato, N. Mizushima, N. Matsumoto, De novo mutations in the autophagy gene WDR45 cause static encephalopathy of childhood with neurodegeneration in adulthood. *Nat. Genet.* **45**, 445–449 (2013).
63. J. Lim, M. Balastik, T. H. Lee, K. Nakamura, Y. C. Liou, A. Sun, G. Finn, L. Pastorino, V. M. Y. Lee, K. P. Lu, Pin1 has opposite effects on wild-type and P301L tau stability and tauopathy. *J. Clin. Investig.* **118**, 1877–1889 (2008).
64. K. Kobayashi, H. Sano, S. Kato, K. Kuroda, S. Nakamuta, T. Isa, A. Nambu, K. Kaibuchi, K. Kobayashi, Survival of corticostriatal neurons by rho/rho-kinase signaling pathway. *Neurosci. Lett.* **630**, 45–52 (2016).
65. K. Tsujikawa, K. Hara, Y. Muro, H. Nakanishi, Y. Niwa, M. Koike, S. Noda, Y. Riku, K. Sahashi, N. Atsuta, M. Ito, Y. Shimoyama, M. Akiyama, M. Katsuno, HMGCR antibody-associated myopathy as a paraneoplastic manifestation of esophageal carcinoma. *Neurology* **87**, 841–843 (2016).

Acknowledgments: We thank the patients and their families for participating in this study. We also thank J. Aoki at Aoki clinic and T. Funahashi at National Hospital Organization Higashi Owari National Hospital for psychological assessment. We thank T. Ando at Department of Neurology, Nagoya University for assistance with microscopic imaging. We thank N. Noguchi and M. Masaoka at Department of Anatomy and Cell Biology, Nagoya University for technical support of IUE. We acknowledge the assistance of Division of Experimental Animals, Nagoya University Graduate School of Medicine for generation of transgenic mouse. **Funding:** This work was supported by KAKENHI grant numbers JP16H02457 and JP17H04195 and

JP20H00527, JP20K07907, and JP20K16932 from the Ministry of Education, Culture, Sports, Science, and Technology (MEXT); grants from Japan Agency for Medical Research and Development (AMED) (nos. JP20ae0101077, JP21dk0207052, JP21ek0109486, JP21ek0109493, JP21ek0109549, JP21wm0425013, JP21wm0425019, JP21wm0525020 JP21dk0207045, and JP21ek0109545); and a grant from The Hori Sciences and Arts Foundation. **Author contributions:** K.T. and M.Katsuno initiated the project. K.T. designed and carried out the experiments. K.T. led data analysis with help from K.S., Y.I., and S.I. T.M., N.S., N.O., and G.S. supervised the project. K.T., S.K., H.K., and K.Y. performed neurological assessment. K.T., Y.M., and G.S. established immortalized LCLs. K.T., Y.R., and M.Y. performed neuropathological assessments. K.T., N.H., and A.H. performed statistical analysis. K.H. and N.H. performed human genome analysis with help from S.Miy., S.Mit., and N.M. K.T. and M.Kats. collected clinical and pathological information for tauopathies with help from T.IK., A.K., Y.S., Y.I., A.M., T.IW., Japanese Alzheimer's Disease Neuroimaging Initiative (J-ADNI), and Japanese Longitudinal Biomarker Study in PSP and CBD (JALPAC) Consortium. Y.H. performed IUE and live imaging for F-actin dynamics. K.T., Y.H., J.L. M.Kata., and Y.I. performed primary culture assay. K.K. prepared AAV. K.T. and Y.I. performed stereotaxic AAV injection for mice brains. K.T. generated original transgenic mice with help from Y.I. and M.Kats. K.T., K.S., Y.R., and M.Kats. interpreted the data and wrote the manuscript with input from all other authors. All authors meet the four International Committee of Medical Journal Editors (ICMJE) authorship criteria. **Competing interests:** K.T., K.S., and M.Kats. are inventors on pending patent applications related to this work filed by National University Corporation Tokai National Higher Education and Research System (PCT patent application no. PCT/JP2021/001026, filed 14 January 2021, published 22 July 2021). The authors declare that they have no other competing interests. **Data and materials availability:** All data needed to evaluate the conclusions in the paper are present in the paper and/or the Supplementary Materials.

Submitted 23 September 2021
Accepted 12 April 2022
Published 25 May 2022
10.1126/sciadv.abm5029